ELSEVIER

Contents lists available at ScienceDirect

Journal of Inorganic Biochemistry

journal homepage: www.elsevier.com/locate/jinorgbio





N-heterocyclic carbene gold(I) derivatives with long aliphatic side chains as potential anticancer agents in colon cancer

Javier Quero ^{a,b,d,e}, Adrián Alconchel ^a, Sara Ortega ^a, Seyed Hesamoddin Bidooki ^{b,c,d,e}, M^a. Concepción Gimeno ^a, M^a. Jesús Rodriguez-Yoldi ^{b,d,e,*}, Elena Cerrada ^{a,**}

- a Instituto de Síntesis Química y Catálisis Homogénea (ISQCH), CSIC–Universidad de Zaragoza, C/ Pedro Cerbuna, 12, 50009 Zaragoza, Spain
- b Departamento de Farmacología y Fisiología, Unidad de Fisiología, Facultad de Veterinaria, Universidad de Zaragoza, 50013 Zaragoza, Spain
- E Departamento de Bioquímica y Biología Molecular y Celular, Facultad de Veterinaria, Universidad de Zaragoza, 50013 Zaragoza, Spain
- d Instituto de Investigaciones Sanitarias de Aragón (IIS Aragón), Instituto Agroalimentario de Aragón, CITA-Universidad de Zaragoza (IA2), E-50013 Zaragoza, Spain
- e CIBER de Fisiopatología de la Obesidad y Nutrición (CIBERobn), Instituto de Salud Carlos III, E-28029 Madrid, Spain

ARTICLE INFO

Keywords: N-heterocyclic carbene Gold Thioredoxin reductase Hyperthermia Colon cancer

ABSTRACT

Mild hyperthermia has emerged as a powerful tool in cancer therapy, prompting the development of materials that respond to heat with enhanced therapeutic action. Gold(I)-NHC complexes are emerging as promising anticancer agents due to their stability, tunability, and ability to inhibit sulfur- and selenium-dependent enzymes overexpressed in tumors. In this study, we synthesised carbene–gold(I) derivatives bearing fluorous and hydrocarbon chains to assess the role of polyfluorinated groups and the impact of mild hyperthermia (41 $^{\circ}$ C) on their cytotoxic activity. The compounds exhibited significant antiproliferative effects against Caco-2/TC7 colon carcinoma cells at both 37 $^{\circ}$ C and 41 $^{\circ}$ C. This activity may be associated with alterations in the levels of ROS (reactive oxygen species) within the cells and the activity of TrxR (thioredoxin reductase), resulting in modifications to the intracellular redox state and subsequent disruptions to the cell cycle. Under hyperthermic conditions, cytotoxicity was further enhanced via mitochondrial depolarization and activation of caspase-3-mediated apoptosis. Notably, fluorinated complexes displayed superior cytotoxicity compared to their alkylated analogues, highlighting the relevance of polyfluorinated chains in boosting therapeutic efficacy under heat-triggered conditions.

1. Introduction

Although there have been significant advancements in cancer screening, prevention, and treatment, the incidence of cancer remains on an upward trend. Due to the increased lifespan, it is anticipated that the incidence of cancer will gradually rise [1]. It has been projected by global statistics that the number of people diagnosed with cancer in 2040 will exceed 27 million per year [2]. Notably, the rise in malignancies, like colorectal, lung and breast cancer, which are frequently untreatable in advanced stages using current therapies, will be a notable factor in this increase [3]. Despite extensive research and the availability of various cancer treatments, conventional methods of treating cancer have several drawbacks, including recurrence and side effects.

Currently, in the particular case of colorectal cancer, the main

adjuvant approaches for patients in advanced stages are chemotherapy and radiotherapy. According to class I recommendations, the preferred clinical options in chemotherapy are either FOLFIRI (fluorouracil combined with irinotecan) or mFOLFOX6 (fluorouracil combined with oxaliplatin) [4]. Both chemotherapy and radiation therapy produce side effects, including nausea, diarrhea, neuropathy, mouth ulcers and even serious liver, kidney and blood system dysfunction [5]. Therefore, exploring and developing new treatments for colorectal cancer is crucial to achieving improved therapeutic results while minimising any negative effects.

Hyperthermia therapy, a noninvasive approach that involves raising the temperature of tumors within the range of 40–45 °C, has emerged as a promising strategy for cancer treatment [6–8]. Hyperthermia is considered a biological sensitiser for radiotherapy and chemotherapy,

E-mail addresses: mjrodyol@unizar.es (Ma.J. Rodriguez-Yoldi), ecerrada@unizar.es (E. Cerrada).

^{*} Correspondence to: M.J. Rodriguez-Yoldi, Departamento de Farmacología y Fisiología, Unidad de Fisiología, Facultad de Veterinaria, Universidad de Zaragoza, 50013 Zaragoza, Spain.

^{**} Corresponding author.

making cancer cells more sensitive to radiation therapy or chemotherapy [6]. Currently, clinical interest in the combination of chemotherapy and hyperthermia is re-emerging due to the publication of several Phase III clinical trials [7–9].

The vasculature architecture in solid tumors is characterised by disorder, leading to areas with low oxygen levels and acidic pH, a phenomenon absent in normal tissues under undisturbed conditions [10]. Cells are particularly susceptible to hyperthermia under these conditions [11]. Hyperthermia can alter crucial tumor growth and survival factors, such as the microenvironment, immune responses, vascularisation, and oxygen supply [12]. The heat from hyperthermia can increase blood flow to the tumor, which can help the chemotherapy drugs reach the cancer cells more effectively and increase the fluidity of phospholipid bilayers in tumor cells, thereby aiding drug permeability through them. Additionally, heat can damage the cancer cells' protective barriers, making them more vulnerable to chemotherapy and increasing the effectiveness of drugs by altering their pharmacokinetics and pharmacodynamics [13].

Combined treatments, chemotherapy and hyperthermia seem to operate through various mechanisms, such as reactive oxygen species (ROS) generation, cell cycle arrest, DNA harm, and mitochondrial membrane potential (MMP) depolarisation. The increased production of ROS within the mitochondria under heat shock conditions causes non-specific alterations of biomolecules, leading to eventual bioenergetic failure [14].

Different types of materials can be used for hyperthermia applications, such as nanomaterials [15,16], thermosensitive liposomes for localised temperature-responsive release of drugs [17] or thermoresponsive fluorinated small molecules [18]. Regarding the last type of materials, examples of perfluorinated derivatives of biologically active molecules such as chlorambucil [19] or SAHA [20] (Suberoylanilide hydroxamic acid), and ruthenium [21,22], platinum [23,24] or gold [25] derivatives with perfluorinated ligands have been activated under mild hyperthermia conditions. These types of thermoresponsive systems undergo structural or chemical changes under mild hyperthermia, enhancing their anticancer effect by improving solubility, shape, or cellular uptake, particularly in ruthenium complexes [21].

In addition, gold complexes have gained significant attraction as promising therapeutic agents for treating various diseases, including rheumatoid arthritis, cancer and microbial infections [26–29]. In this context, one of the most extensively studied classes of gold-based drugs

is based on the N-heterocyclic carbene (NHC) donor motif. This is due to their well-established stability even in physiological environments, along with the ease of synthesis via modification of the NHC moiety. Properly designed Au(I)-NHC complexes have demonstrated promising anticancer potential [30–33]. These derivatives can selectively bind to biological sulfur- and selenium-containing amino acids, inhibiting essential enzymes like thioredoxin reductase, glutathione reductase, and cysteine proteases, which are overexpressed in cancer cells [34–36].

With this background, we describe the synthesis of carbene gold derivatives bearing either fluorous or hydrocarbon side chains, designed to explore the impact of polyfluorinated moieties under mild hyperthermia conditions. The cytotoxicity of these new compounds was assessed against human colon carcinoma (Caco-2) at 37 $^{\circ}\text{C}$ and compared to a hyperthermic treatment regimen at 41 $^{\circ}\text{C}$ (1 h at 41 $^{\circ}\text{C}$ followed by 71 h of incubation at 37 $^{\circ}\text{C}$). Their potential intracellular targets were also investigated, including TrxR inhibition, mitochondrial disturbances and apoptotic implications.

2. Results and discussion

2.1. Synthesis and characterisation of the NHC-Au complexes

The reaction of N-benzyl or N-pyridyl imidazole with 1-iodooctane in toluene under reflux gave the corresponding imidazolium salts 1a-b as brown oils in good yields (Scheme 1). In their ¹H NMR spectra, the resonance for the NCHN imidazolium proton at around 11 ppm in addition to the phenyl, pyridine and aliphatic chain signals confirms their formation. In the ¹³C{¹H} NMR spectra, the resonance due to the C-2 atom is observed at around 133 ppm, which agrees with previously reported data for imidazolium salts [37]. Using 1H,1H,2H,2H-Perfluoro-1-iodooctane did not afford the corresponding polyfluorinated imidazolium salts (3a-b). Instead, we synthesised the more reactive alkyl triflate TfOCH2CH2(CF2)5CF3 (2) (see experimental) which led to the preparation of [(IPyOctF)H]TfO (3a) and [(IPyOctF)H]TfO (3b) (OctF $= -(CH_2)_2C_6F_{13}$) as white solids in high yield. Their ¹H NMR spectra are similar to those observed for 1a-b salts. However, only the methylene groups α and β to the N atom are visible in the spectra in a downfield displacement due to the polyfluorinated chain. Their IR, ¹⁹F{¹H} NMR and ¹³C{¹H} NMR spectra gave additional evidence for the N-perfluorinated alkylation, showing the corresponding bands to C-F bonds, the signals due to the -(CF₂)₅CF₃ chain and multiplets in the region of

i) n-Bul, reflux, 24h; ii) Rf(TfO), 24h; iii) Ag_2O , 4h; iv) [AuCl(tht)], 4h; v) $NBu_4(acac)$ + [AuCl(tht)], 24h vi) Cs_2CO_3 + HSPy, 4h

Scheme 1. Synthesis of the imidazolium salts and carbene derivatives

122-114 ppm assigned to 6C of the perfluorinated chain, respectively.

The reaction of the imidazolium salts 1a-b with silver oxide afforded the new silver(I) derivatives [AgI(IROct)] (R = Py (4a), Bn (4b)), as shown in Scheme 1. Coordination of silver atom and formation of the carbene species is confirmed by the disappearance of the C2—H (NCHN) imidazolium proton in the ¹H NMR spectra and the downfield shift of the carbene carbon atom nuclei in their ¹³C{¹H} NMR spectra, in addition to the presence of peaks with m/z that correspond to $[M-I]^+$ in their mass spectra. No related silver compounds with the perfluorinated chains were isolated via Ag₂O reaction, and mixtures of unreacted starting materials were detected in the reaction medium. Carbene transfer reactions from the silver complexes with [AuCl(tht)] provided the corresponding carbene gold(I) derivatives [AuCl(IROct)] (R = Py (5a), Bn (5b), scheme 1). A similar pattern to that of the silver precursor is observed in the ¹H NMR and ¹³C{¹H} NMR spectra of **5a** and **5b**, in addition to the vibration $\nu(Au-Cl)$ in their IR spectra. Peaks at m/z 711 and 737 corresponding to the more stable cation [Au(IOctR)₂]⁺ are detected in their mass spectra (ESI⁺). The preparation of the counterparts with the polyfluorinated appendage **6a** and **6b** was afforded by the reaction of the imidazolium salts 3a-b with NBu4(acac) as a deprotonating agent in the presence of [AuCl(tht)], which has been previously proved as an efficient method for the synthesis of NHC gold complexes

The addition of mercaptopyridine in the presence of Cs_2CO_3 to the chloro carbene precursors **5–6 (a-b)** afforded the corresponding thiolate derivatives **7–8 (a-b)** as shown in Scheme 1. These thiolate derivatives display resonances in their 1H NMR spectra due to the NHC ligand and the SPy unit, which are highfield displaced. In their $^{13}C\{^1H\}$ NMR spectra, a high field displacement of about 15 ppm is observed for the resonances of the carbene carbon atoms compared to the parent chloride complexes. Besides, the disappearance of the $\nu(Au-Cl)$ in their IR spectra points to the coordination of the thiolate moiety.

Bis-carbene gold(I) complexes 10-11(a-b) (Scheme 2) were efficiently synthesised using Cs_2CO_3 as a base. The polyfluorinated derivatives were obtained from imidazolium salts 3a and 3b, while the corresponding hydrocarbon analogues were prepared from salts 9a and 9b, which were in turn derived from 1a and 1b via metathesis with AgBF₄ (see Experimental Section). These new derivatives display the signals of the anions BF_4^- or TfO^- in their $^{19}F\{^1H\}$ NMR, similar pattern in their ^{14}H and $^{13}C\{^1H\}$ NMR spectra to that found in the imidazolium salts with an upfield shift of the imidazole protons and a downfield displacement of the C-2 (NCN) resonance to the region of about 180 ppm

in addition to the molecular ion peaks [M]⁺ in their mass spectra.

We have studied the solution stability of the new complexes under physiological conditions, by dissolving them in phosphate-buffered saline (PBS) at pH 7.4 and maintaining at 37 $^{\circ}$ C for 24 h. The UV–vis absorption spectrum of each complex was recorded at different time intervals (fig. S51). These spectra display bands in the range of 200–300 nm due to the ligands, which undergo slight hypochromic shifts over time, being more affected in the case of complexes 5a, 8a and 11b. Neither band shifts nor additional bands characteristic of metallic gold formation are detected during the time experiment. In addition, neither decomposition nor precipitation is observed along the time, which shows that the complexes are essentially stable for at least 24 h in PBS solution at 37 $^{\circ}$ C.

Lipophilicity plays a crucial role in cancer research and treatment due to its impact on drug delivery, cellular uptake, and overall efficacy of anticancer agents. It is believed to play a significant role in the passive influx of drug molecules into cells, since they can cross into and go through the cell walls more easily, allowing them to reach target sites in the body, including cancer cells [39].

We attempted to determine the hydrophilicity of these complexes (logP value) by the shake-flask n-octanol/water partitioning method (Table 1). Incorporation of long polyfluorinated side chains in

Table 1 Distribution coefficients and IC_{50} (μM)^a values obtained following 72 h treatment at 37 °C or 1 h at 41 °C followed by 71 h at 37 °C with the complexes on undifferentiated Caco-2/TC7 cells.

Complex	logP _{7.4}	IC ₅₀ (μM)	
		37 °C	41 °C
[AuCl(IPyOct)] (5a)	0.42	1.79 ± 0.55	2.65 ± 0.16
[AuCl(IBnOct)] (5b)	1.20	0.51 ± 0.16	0.32 ± 0.16
[AuCl(IPyOct-F)] (6a)	0.16	2.39 ± 0.19	3.58 ± 1.57
[AuCl(IBnOct-F)] (6b)	0.25	2.61 ± 0.30	1.85 ± 0.17
[Au(SPy)(IPyOct)] (7a)	0.52	1.56 ± 0.31	5.49 ± 1.10
[Au(SPy)(IBnOct)] (7b)	1.00	1.08 ± 0.04	0.72 ± 0.02
[Au(SPy)(IPyOct-F)] (8a)	0.32	1.60 ± 0.27	3.91 ± 0.34
[Au(SPy)(IBnOct-F)] (8b)	0.25	1.66 ± 0.18	1.39 ± 0.20
$[Au(IPyOct)_2]BF_4$ (10a)	0.42	0.09 ± 0.01	1.23 ± 0.11
$[Au(IBnOct)_2]BF_4$ (10b)	0.15	0.44 ± 0.21	2.2 ± 0.01
$[Au(IPyOct-F)_2]BF_4$ (11a)	0.46	0.46 ± 0.15	0.65 ± 0.09
[Au(IBnOct-F) ₂]BF ₄ (11b)	0.47	1.42 ± 0.27	3.08 ± 0.06

 $^{^{\}rm a}$ Mean \pm SE of at least three determinations.

i) AgBF₄; ii) Cs₂CO₃ + [AuCl(tht)]

Scheme 2. Preparation of bis-carbene gold(I) derivatives.

complexes of the general formula [AuX(IRR')] confers decreased lipophilicity to the overall structure. Thus, carbene complexes with the polyfluorinated side chains **6a**, **6b**, and **8a**, **8b** lead to lower logP values than their counterparts.

2.2. Biological studies

2.2.1. Cytotoxic effect of gold complexes

The anticancer potential of these novel gold(I) derivatives was assessed using the human carcinoma cell line Caco-2. The cytotoxic effect of the gold complexes on these cells was determined by calculating IC_{50} values (concentration of the compound required to inhibit 50 % of cell growth in vitro) after 72 h incubation of the cells under two different conditions (one for 72 h at 37 $^{\circ}$ C, and the other for 1 h at 41 $^{\circ}$ C followed by 71 h at 37 °C). The obtained IC₅₀ values, summarised in Table 1, indicate a high activity against colon cancer cells, ranging from 0.09 to $2.61~\mu M$ after incubation at 37 °C. Most values are in the range of similar carbene gold(I) derivatives [40–43]. Notably, the most active complexes are 5b and the bis-carbene 10a, 10b and 11a, with complex 10a standing out as its IC₅₀ value is approximately five times lower. Only mono-carbene complexes with the benzyl substituent suffered a decrease in the IC_{50} value when cells were incubated at 41 °C for 1 h. The remaining complexes exhibit similar or slightly lower cytotoxicity at higher temperatures. However, the perfluorinated chain in the complexes did not entail significant differences in the IC50 values compared to the alkylated counterparts.

A non-linear relationship was observed between the lipophilic nature of the compounds and their cytotoxic activity after incubation at 37 $^{\circ}$ C. As the lipophilic character increased, as indicated by higher log p values, the activities of the complexes displayed an inverted U-shaped curve (Fig. S52, Supplementary). Based on this correlation, derivatives with ligands that can afford intermediate logP values, approximately 0.6, could exhibit the highest anticancer activity.

On the other hand, the relationship between lipophilic character and cytotoxicity after incubation at 41 $^{\circ}$ C for 1 h shows an upward curve. With this result, we can expect a greater cytotoxic effect with those complexes that are more lipophilic. Complex **5b** is the clearest example since it is both more lipophilic and more cytotoxic.

The complexex [Au(SPy)(IBnOct)] (7b) and its perfluorinated counterpart [Au(SPy)(IBnOct-F)] (8b) exhibit low IC $_{50}$ values at 37 °C, indicating high potency under normothermic conditions. These values are further reduced under mild hyperthermia conditions, suggesting enhanced activity. Based reason these promising results, both compounds were selected for further evaluation, including toxicity assessment in two non-cancerous cell models, AML12 mouse liver cells and differentiated human Caco-2 cells (Table 2), and investigation of their mechanism of action in cancerous human Caco-2 cells.

The cancerous Caco-2 cell line is widely used as an in vitro model of the small intestinal epithelium, as it mimics the intestinal barrier due to

Table 2 IC $_{50}$ (µM) 8 values obtained following 72 h treatment at 37 °C or 1 h at 41 °C followed by 71 h at 37 °C with the complexes on the non-cancerous differentiated Caco-2/TC7 and AML12 cells compared with undifferentiated Caco-2/TC7 (cancerous cells) and their corresponding selectivity index.

Cells	T	[Au(SPy)(IBnOct)] (7b)	[Au(SPy)(IBnOct-F)] (8b)
Undifferentiated	37 °C	1.08 ± 0.04	1.66 ± 0.18
Caco-2	41 °C	0.72 ± 0.02	1.39 ± 0.20
Differentiated	37 °C	22.04 ± 0.07	19.27 ± 0.01
Caco-2	41 °C	17.04 ± 0.16	19.06 ± 0.09
AML12	37 °C	5.25 ± 0.01	18.08 ± 0.12
	41 °C	4.62 ± 0.01	15.89 ± 0.11
SI	37 °C	20.41 (4.86)	11.61 (10.89)
	41 °C	23.67 (6.42)	13.71 (11.43)

 $[^]a$ Mean \pm SE of at least three determinations SI = IC $_{50}$ differentiated Caco-2/ IC $_{50}$ undifferentiated Caco-2 (IC $_{50}$ AML12/IC $_{50}$ undifferentiated Caco-2).

the spontaneous differentiation acquired after reaching confluence. At this stage, the cells present a structure of brush border on the apical surface with tight junctions. This brush border resembles that observed in healthy human small-intestinal tissue, expressing also the same hydrolases, nutrient transporters, bacterial receptors, and other proteins present in enterocytes [44].

As shown in Table 2, both compounds [Au(SPy)(IBnOct)] (7b) and [Au(SPy)(IBnOct-F)] (8b) display selective cytotoxicity towards undifferentiated Caco-2 cells, which are representative of a cancerous phenotype, with significantly lower IC_{50} values compared to differentiated Caco-2 and AML12 cells, which model non-cancerous intestinal and liver cells respectively. Among the two, complex 7b shows superior potency and selectivity, particularly under mild hyperthermia, where its selectivity index (SI) reaches 23.67 in colon cells. Although compound 8b is less cytotoxic overall, it exhibits a more favourable safety profile in healthy cells, especially AML12, suggesting broader therapeutic tolerance.

Overall, our results support the use of mild hyperthermia to improve the selectivity and therapeutic window of both complexes, showing their potential as promising anticancer agents, especially compound **7b**, making it a promising candidate for further development.

2.2.2. Studies of cellular death (apoptosis, mitochondrial potential, caspase 3 and cell cycle)

Since the studied complexes inhibited cell proliferation, various flow cytometry analyses were conducted to determine the type of cell death induced by these gold compounds in Caco-2 cells. Additionally, these analyses aimed to confirm the previously suggested influence of temperature and perfluorinated chains on the cytotoxic capacity of the complexes.

Double staining with Annexin V/PI revealed that the selected two gold compounds [Au(SPy)(IBnOct)] (**7b**) and the counterpart [Au(SPy) (IBnOct-F)] (**8b**) induced apoptosis in Caco-2 cells after 1 h incubation at 41 $^{\circ}$ C, followed by 23 h at 37 $^{\circ}$ C. Conversely, the compounds showed no detectable effect on the cells after 24 h incubation at 37 $^{\circ}$ C (Fig. 1a).

Mitochondrial depolarisation is one of the first steps in apoptosis. During this process, mitochondria undergo a redistribution of hydrogen ions, leading to a decrease in $\Delta\Psi m$. This decrease triggers a cascade of structural changes that ultimately lead to the release of cytochrome c. DilC1(5) staining showed that complexes **7b** and **8b** induced mitochondrial depolarisation in Caco-2 cells pre-treated for 1 h at 41 °C. Specifically, under these conditions, the proportion of cells exhibiting changes in mitochondrial membrane potential—namely, a reduction in $\Delta\Psi m$ —increased significantly (Fig. 1b).

Mitochondrial depolarisation and cytochrome c release ultimately lead to caspase-3 activation, which initiates the apoptotic process. Flow cytometry analysis confirmed the above findings, as cells incubated with both gold complexes and exposed to high temperature (41 °C) for 1 h exhibited a higher percentage of cells with active caspase-3 (Fig. 1c). These results suggest that complexes 7b and 8b may undergo structural modifications at elevated temperatures, likely through increased cell internalisation, which activates caspase-3 following $\Delta\Psi m$ reduction, consequently triggering apoptosis in Caco-2 cells.

Cell antiproliferative events are often associated with disruptions in the cell cycle. Previous studies on gold derivatives have suggested that treated cells may experience cell cycle arrest at various checkpoints, hindering their progression through different phases [45–47].

Flow cytometry analyses revealed that, after 24 h of incubation with complexes **7b** and **8b**, normal cell cycle progression was disrupted, regardless of temperature. In particular, complex **7b** induced an accumulation of cells in G2/M phase, accompanied by a corresponding decrease in the S-phase population (Fig. 2). Compound **8b**, on the other hand, caused an increase in the number of cells in S phase and a decrease in the number of cells in G0/G1 phase under the two temperature conditions tested. It can therefore be concluded that the impact of these complexes on the cell cycle is primarily driven by their structural

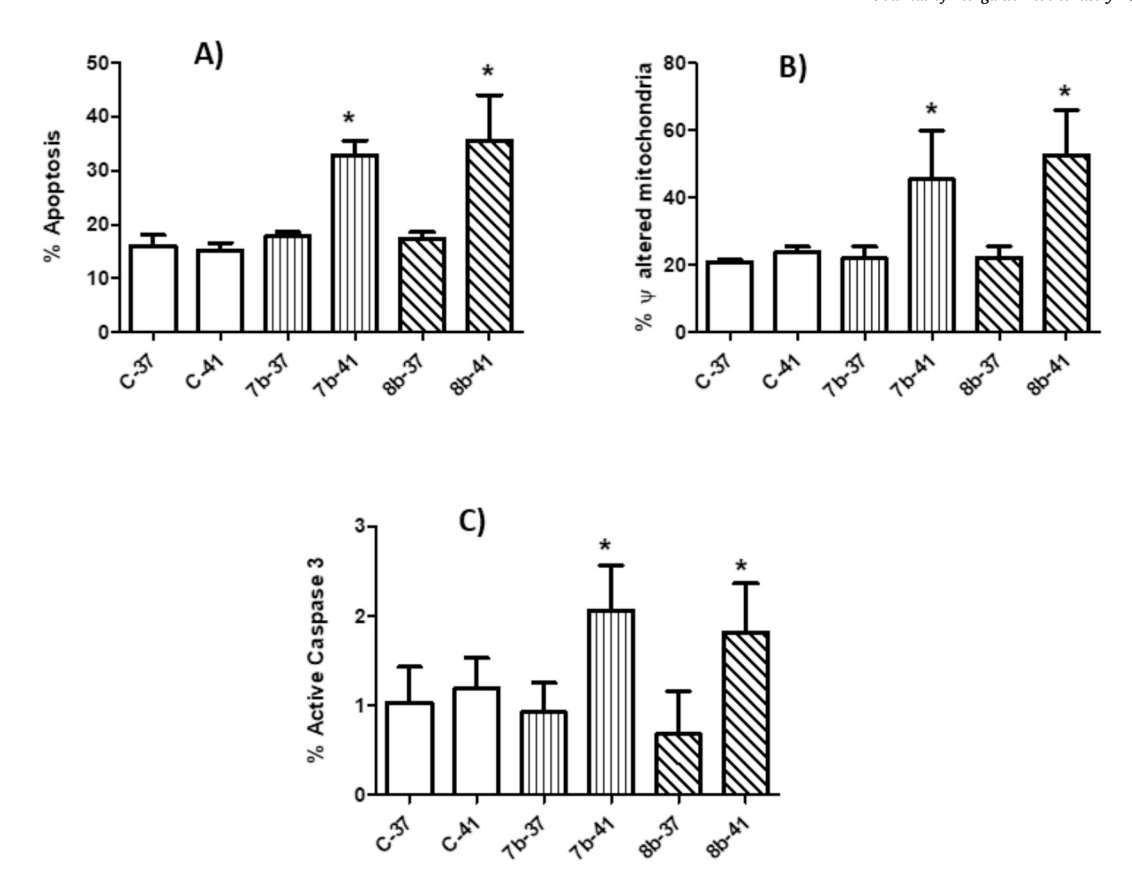


Fig. 1. (A) Analysis of apoptosis, (B) mitochondrial membrane potential and (C) caspase 3 activities after 24 h incubation time with 7b and 8b at IC₅₀ (1.08 and 1.66 μ M, respectively) at 37 °C (C-37; 7b-37 and 8b-37) or 1 h incubation at 41 °C followed by 23 h at 37 °C (C-41; 7b-41 and 8b-41). *p < 0.05 vs control (untreated cells) at respective temperature.

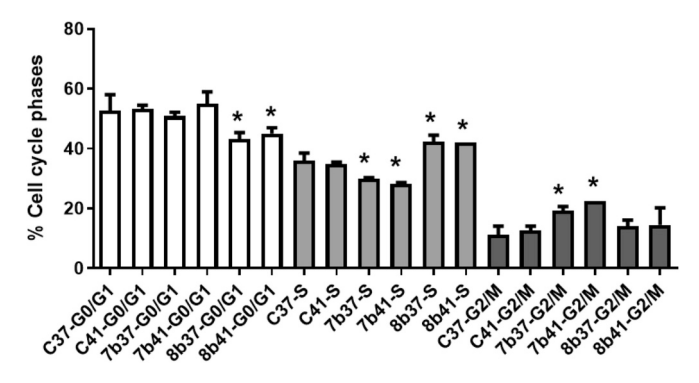


Fig. 2. Percentage of cells in different phases of the cell cycle after 24 h incubation time with **7b** and **8b** at IC $_{50}$ (1.08 and 1.66 μ M, respectively) at 37 °C (C-37; 7b-37 and 8b-37) or 1 h incubation at 41 °C followed by 23 h at 37 °C (C-41; 7b-41 and 8b-41).*p < 0.05 vs control (untreated cells) at respective temperature.

properties rather than temperature.

Throughout the cell cycle, cells pass through different checkpoints that ensure the order, integrity and fidelity of previous events before progressing through the cell cycle to the next phase [48]. Perhaps this could explain why these complexes take longer to act on cells at 37 $^{\circ}\text{C}.$ Consequently, a short incubation at 41 $^{\circ}\text{C}$ appears essential to accelerate their effect on Caco-2 cancer cells.

2.2.3. Studies of redox balance (ROS intracellular levels and analysis of thioredoxin activity

Previous studies on gold derivatives have demonstrated disruptions

in the ROS balance when cancer cells are treated with these metal complexes [49,50], typically leading to an increase in intracellular ROS levels. This effect is attributed to the ability of various gold(I) derivatives to interact with thioredoxin reductase (TrxR), thereby inhibiting its antioxidant activity [27], since this enzyme serves as a crucial regulator in maintaining cellular redox homeostasis [51,52]. Besides, TrxR is frequently overexpressed in primary human cancers, including breast cancer, thyroid, prostate and colorectal carcinoma, and malignant melanoma [53]. Therefore, to investigate the effect of intracellular ROS levels and TrxR activity by both gold complexes 7b and 8b, these parameters in Caco-2 cells after incubating at 37 °C or 41 °C were examined. The results of our study demonstrated a substantial alteration in the intracellular ROS levels of cells treated with complexes 7b and 8b. A considerable augmentation in ROS levels was detected upon a 24 h treatment with IC50 values at 37 °C; however, a marked reduction in ROS was observed in cells exposed to 41 °C (Fig. 3A). Interestingly, this temperature-dependent shift in ROS levels corresponded with changes in TrxR activity. Specifically, both 7b and 8b compounds exhibited an inhibitory effect on TrxR after 24 h of incubation at 37 °C. In contrast, following a brief 1 h exposure to 41 °C and subsequent 23 h incubation at 37 °C, both compounds led to an increase in TrxR enzyme activity (Fig. 3B).

At 37 °C, these compounds reduce the proliferation of cancer cells by disrupting the redox balance through decreased thioredoxin reductase activity, which affects the cell cycle. However, elevated temperature (41 °C for 1 h) may facilitate the cellular uptake of the complexes and concomitantly augment cellular metabolic activity. This leads to increased activity of the enzymes thioredoxin reductase and caspase-3, resulting in cell death through apoptosis.

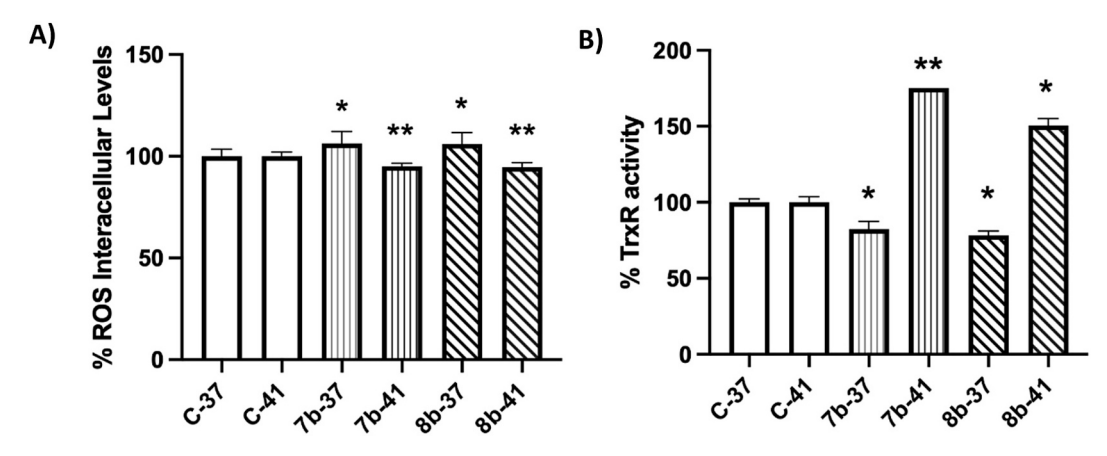


Fig. 3. (A) Measurements of ROS intracellular levels and (B) determination of TrxR activity after 24 h incubation time with 7b and 8b at IC $_{50}$ (1.08 and 1.66 μ M, respectively) at 37 °C (C-37; 7b-37 and 8b-37) or 1 h incubation at 41 °C followed by 23 h at 37 °C (C-41; 7b-41 and 8b-41). *p < 0.05, **p < 0.01 vs control (untreated cells) at respective temperature.

3. Conclusions

The newly synthesised gold(I) carbene complexes, bearing both fluorous and hydrocarbon substituents, demonstrated potent antiproliferative activity against human colon carcinoma cells (Caco-2/ TC7), under both normothermic (37 °C, 72 h) and mild hyperthermic (41 °C for 1 h followed by 71 h at 37 °C) conditions. Notably, the complexes [Au(SPy)(IBnOct)] (7b) and its perfluorinated analogue [Au (SPy)(IBnOct-F)] (8b) exhibited significant cytotoxicity, likely mediated by inhibition of thioredoxin reductase (TrxR), leading to an intracellular redox imbalance caused by elevated levels of reactive oxygen species (ROS), ultimately resulting in cell cycle disruption. Although only a slight difference in IC₅₀ values is observed under mild hyperthermia conditions in these complexes, this modest change results in a significant biological effect, as evidenced by caspase-3 activation and enhanced mitochondrial depolarisation, ultimately leading to a marked increase in apoptosis-mediated cell death. In addition, both complexes exhibit promising selective cytotoxicity against cancer cells, as evidenced by their reduced toxicity in non-cancerous cell models and enhanced activity under mild hyperthermia. Compound 7b, in particular, stands out for its high potency and selectivity, supporting its potential for further development as an anticancer agent.

These findings underscore the thermosensitive nature of the compounds and highlight the synergistic potential of gold(I) therapeutics when combined with localised hyperthermia.

Moreover, the presence of perfluorinated chains appeared to have a limited impact on cellular viability, since such fluorinated complexes exhibited $\rm IC_{50}$ values comparable to those of the hydrocarbon counterpart. This fact indicates that, while fluorination may influence the physicochemical properties of the compounds, no significant biological activity enhancement was observed.

4. Materials and methods

4.1. General procedures

All reactions were performed under an air atmosphere, and solvents were used as received without purification or drying. The starting materials [AuCl(tht)][54], 2-(1H-imidazol-1-yl)pyridine[55], NBu₄(acac) [38] were prepared according to published procedures. All other reagents are commercially available. $^{1}\mathrm{H}$, $^{13}\mathrm{C}\{^{1}\mathrm{H}\}$, and $^{19}\mathrm{F}\{^{1}\mathrm{H}\}$ NMR, were recorded at room temperature on a BRUKER AVANCE 400 spectrometer ($^{1}\mathrm{H}$ 400 MHz; $^{13}\mathrm{C}$, 100.6 MHz; $^{19}\mathrm{F}$ 377 MHz) or on a BRUKER AVANCE II 300 spectrometer ($^{1}\mathrm{H}$ 300 MHz; $^{13}\mathrm{C}$ 75.5 MHz; $^{19}\mathrm{F}$ 282 MHz) with chemical shifts (δ , ppm) reported relative to the solvent peaks of the deuterated solvent. Mass spectra were recorded on a BRUKER ESQUIRE

3000PLUS, with the electrospray (ESI) or MALDI techniques. A Bruker MicroToF-Qspectrometer was used for high-resolution mass spectra-ESI (HRMS-ESI) equipped with an API-ESI source and a QTOFmass analyser.

4.2. Synthesis of imidazolium salts

4.2.1. Synthesis of [(IROct)H]I

2-(1H-imidazol-1-yl)pyridine or 1-benzylimidazole (1 mmol) were added to a solution of iodooctane (1 mmol) in toluene (15 mL). Then, the solution was refluxed for 24 h with stirring. After cooling, the solution was evaporated to dryness leading to brown oils.

[(IPyOct)H]I (1a). Yield: 94 %. ¹H RMN (400 MHz, CDCl₃, δ (ppm): 11.41 ("t", 1H, Im), 8.58–8.54 (m, 1H, Py), 8.54–8.51 (m, 1H, Py), 8.30 (t, $J_{HH} = 1.8$ Hz, 1H, Im), 8.06 (ddd, $J_{HH} = 8.2$; 7.5; 1.8 Hz, 1H, Py), 7.50–7.43 (m, 2H, Py + Im), 4.58 (t, $J_{HH} = 7.2$ Hz, 2H, CH_2 -N), 2.10–1.96 (m, 2H, CH_2 -CH₂-N), 1.48–1.17 (m, 10H, -CH₂-), 0.86 (t, $J_{HH} = 8$ Hz, 3H, CH₃). ¹³C{¹H}-APT RMN (75.5 MHz, CDCl, δ (ppm)): 148.9 (Py), 145.7 (Py), 140.49 (Py), 134.5 (Im), 125.2 (Py), 122.6 (Im), 121.9 (Im), 114.9 (Py), 50.7 (CH₂), 31.5 (CH₂), 30.2 (CH₂), 28.9 (CH₂), 28.9 (CH₂), 26.1 (CH₂), 22.5 (CH₂), 13.9 (CH₃) MS (MALDI+): m/z (%) = 258.1 (100 %) [M-I]+. HRMS (ESI-QTOF) m/z: [M - I]+ calcd for C₁₆H₂₄N₃, Exact Mass: 258.1965; found, 258.1986.

[(IBnOct)H]I (**1b**). Yield: 97 %. 1 H RMN (400 MHz, CDCl₃, δ (ppm)): 10.43 (s, 1H, Im), 7.53–7.45 (m, 2H, Ph), 7.44–7.36 (m, 3H, Ph), 7.25(s, 1H, Im), 7.23 (s, 1H, Im), 5.60 (s, 2H, N- CH_2 -Ph), 4.29 (t, 2H, J_{H-H} = 7.5 Hz, CH_2 -N), 2.01–1.86 (m, 2H, CH_2 -CH₂-N), 1.41–1.16 (m, 10H, -CH₂-), 0.86 (t, J_{H-H} = 8 Hz, 3H, CH₃). 13 C(1 H)c-APT RMN (75.5 MHz, CDCl₃, δ (ppm)): 132.7 (Im), 129.1 (Ph), 129.3 (Ph), 128.9 (Ph), 122.15 (Im), 122.05 (Im), 53.1 (CH₂), 50.2 (CH₂), 31.5 (CH₂), 30.0 (CH₂), 28.9 (CH₂), 28.7 (CH₂), 26.1 (CH₂), 22.4 (CH₂), 13.9 (CH₃). MS (MALDI⁺): m/z (%) = 271.2 (100 %) [M-I]⁺. HRMS (ESI-QTOF) m/z: [M - I]⁺ calcd for C₁₇H₂₇N₂, Exact Mass: 271.2169; found, 271.2179.

4.2.2. Synthesis of [RfOTf] (2) $(R_f = -(CH_2)_2C_6F_{13})$

1H,1H,2H,2H-perfluorooctanol (5 mmol) and pyridine (5 mmol) in dry dichloromethane (15 mL) were cooled at -78 °C under inert atmosphere. A solution of trifluoromethanesulfonic anhydride (7,50 mmol) in dichloromethane was added dropwise. After 3 h of stirring, the reaction was allowed to reach room temperature. Water (10 mL) was then added, followed by dichloromethane (10 mL). The reaction solution was washed with water and dried over MgSO₄ anhydrous. The solvent was evaporated and the crude was then eluted with dichloromethane on silica gel to afford a colourless oil in 81 % yield. ¹H RMN (400 MHz, CDCl₃, δ (ppm)): 4.72 (t, $J_{H-H} = 6.3$, 2H, CH_2 -O-), 2.80–2.55 (m, 2H, CH₂). ¹⁹F{¹H} RMN (377 MHz, CDCl₃, δ (ppm)): -74.64 (s, 3F, TfO) -80.84 (tt, $J_{F-F} = 9.9$, $J_{F-F} = 2.3$ Hz, 3F, CF₃), -113.54 (m, 2F, CF₂),

-121.83 (m, 2F, CF₂), -122.87 (s, 2F, CF₂), -123.46 (m, 2F, CF₂), -126.14 (m, 2F, CF₂).

4.2.3. Synthesis of $[(IRR_f)H]TfO (R_f = OctF = -(CH_2)_2C_6F_{13})$

2-(1H-imidazol-1-yl)pyridine or 1-benzylimidazole (1 mmol) were added to a solution of [R $_{\rm f}$ OTf] (1.1 mmol) in dichloromethane (15 mL). Then, the solution was stirred for 24 h and the solution was reduced to minimum volume under vacuum. A white solid precipitated and washed with diethyl ether.

[(IPyOctF)H]TfO (3a). Yield: 95 %. 1 H RMN (400 MHz, CDCl₃, δ (ppm)): 10.16 (s, 1H, Im), 8.55 (m, 1H, Py), 8.29 ("t", 1H, Im), 7.08–8.00 (m, 2H, Py), 8.68 ("t", 1H, Im), 7.50–7.47 (m, 1H, Py), 4.87 (t, 2H, $J_{H-H} = 7.5$ Hz, CH_2 -N), 2.98–2.86 (m, 2H, CH_2 -CH₂-N), 13 C{ 1 H}-APT RMN (75.5 MHz, CDCl₃, δ (ppm)): 149.1 (Py), 145.8 (Py), 140.4 (Py), 134.8 (Im), 125.4 (py), 123.8 (Im), 119.3 (Im), 122.0–110 (m series, 6C, -CH₂-CF₂-CF₂-, -CH₂-CF₂-CF₂-, -CH₂-(CF₂)₃-CF₂-, -CH₂-(CF₂)₄-CF₂-, -CH₂-(CF₂)₃-CF₂-, -CH₂-(CF₂)₄-CF₂-CF₃), 42.9 (CH_2 CH₂-R_f), 31.3 (CH_2 CH₂-R_f). CH_2 RHRMN (377 MHz, CDCl₃, δ (ppm)): CH_2 CH₂-R_f), $CH_$

[(IBnOctF)H]TfO (3b). Yield: 96 %. 1 H RMN (400 MHz, CDCl₃, δ (ppm)): 9.42 (s, 1H, Im), 7.44–7.33 (m, 6H, pH + Im), 7.13 ("t", 1H, Im), 5.37 (s, 2H, N- CH_2 -Ph), 4.64 (t, $J_{H-H}=6.6$, 2H, CH_2 -N), 2.94–2.73 (m, 2H, CH_2 -CH₂-N). 13 C{ 1 H}-APT RMN (75.5 MHz, CDCl₃, δ (ppm)): 132.1 (Im), 129.7 (Ph), 129.5 (Ph), 128.9 (Ph), 122.7 (Im), 121.9 (Im), 122.0–114.1 (m series, 6C, -CH₂- CF_2 -CF₂-, -CH₂- CF_2 -CF₂-CF₂-CF₂-, -CH₂-(CF₂)₃- CF_2 -, -CH₂-(CF₂)₄- CF_2 -CF₃, 53.8 (CH_2 -Ph), 42.4 (CH₂), 31.3 (CH₂). 19 F{ 1 H} RMN (377 MHz, CDCl₃, δ (ppm)): -78.75 (s, 3F, TfO), -80.81 (t, $J_{FF}=9.8$, 3F, CF₃), -113.70 (m, 2F, CF₂), -121.87 (m, 2F, CF₂), -122.87 (s, 2F, CF₂), -123.43 (m, 2F, CF₂), -126.17 (m, 2F, CF₂). (MALDI⁺): m/z (%) = 505.1 (100 %) [M-TfO]⁺. Anal. Calcd (%) for C₁₉H₁₄F₁₆N₂O₃S (654.36): C, 34.87; H, 2.16; N, 4.28; S, 4.90. Found: C, 35.32; H, 2.45; N, 4.43; S, 4.86.

4.2.4. Synthesis of [(IROct)H]BF4

AgBF4 (0.25 mmol) was added to a solution of 1a or 1b (0.25 mmol) in dichloromethane/methanol (10 mL/2 mL). The mixture was protected from light and stirred for 2 h at room temperature. Then the solution was filtered through Celite and the solution was reduced to minimum volume under vacuum. A white solid was obtained and washed with diethyl ether.

[(IPyOct)H]BF₄ (9a). Yield: 89 %. H RMN (400 MHz, CDCl₃, δ (ppm): 9.91 ("t", 1H, Im), 8.52 (ddd, $J_{H\cdot H}=4.8$; 1.8; 0.8 Hz, 1H, Py), 8.26 (t, $J_{H\cdot H}=1.9$ Hz, 1H, Im), 8.13 (dt, $J_{H\cdot H}=8.3$; 0.8 Hz, 1H, Py), 8.05 (ddd, $J_{H\cdot H}=8.3$; 7.5; 1.8 Hz, 1H, Py), 7.49–7.46 (m, 2H, Py + Im), 4.43 (t, $J_{H\cdot H}=7.4$ Hz, 2H, CH_2 -N), 1.98–1.94 (m, 2H, CH_2 -CH₂-N), 1.40–1.20 (m, 10H, -CH₂-), 0.86 (t, $J_{H\cdot H}=6.9$ Hz, 3H, CH₃). 19 F{¹H} RMN (377 MHz, CDCl₃, δ (ppm)): -148.24. 13 C{¹H}-APT RMN (75.5 MHz, CDCl, δ (ppm)): 149.2 (Py), 145.7 (Py), 140.6 (Py), 133.3 (Im), 125.8 (Py), 123.6 (Im), 119.3 (Im), 114.0 (Py), 50.8 (CH₂), 31.6 (CH₂), 30.1 (CH₂), 29.0 (CH₂), 28.9 (CH₂), 26.1 (CH₂), 22.5 (CH₂), 14.0 (CH₃). MS (MALDI+): m/z (%) = 258.2 (100 %) [M-BF₄]+

[(IBnOct)H]BF₄ (**9b**). Yield: 92 %. ¹H RMN (400 MHz, CDCl₃, δ (ppm)): 8.92 (s, 1H, Im), 7.32–7.30 (m, 5H, Ph), 7.18 (s, 1H, Im), 7.16 (s, 1H, Im), 5.27 (s, 2H, N-CH₂-Ph), 4.09 (t, 2H, $J_{H-H} = 7.4$ Hz, CH_2 -N), 1.78 (m, 2H, CH_2 -CH₂-N), 1.22–1.16 (m, 10H, -CH₂-), 0.79 (t, $J_{H-H} = 6.8$ Hz, 3H, CH₃). ¹⁹F{¹H} RMN (377 MHz, CDCl₃, δ (ppm)): -148.24. ¹³C{¹H}-APT RMN (75.5 MHz, CDCl₃, δ (ppm)): 135.9 (Im), 132.8 (Ph), 129.5 (Ph), 128.0 (Ph), 120.8 (Ph), 122.1 (Im), 122.0 (Im), 53.5 (CH₂), 50.2 (CH₂), 31.6 (CH₂), 30.0 (CH₂), 29.0 (CH₂), 28.8 (CH₂), 26.2 (CH₂), 22.6 (CH₂), 14.0 (CH₃). MS (MALDI⁺): m/z (%) = 271.2 (100 %) [M-BF₄]⁺. Anal. Calcd (%) for C₁₈H₂₇BF₄N₂ (358.23): C, 60.35; H, 7.60; N, 7.82. Found: C, 60.43; H, 7.88; N, 7.82.

4.3. Synthesis of silver derivatives

4.3.1. Synthesis of [AgI(IROct)]

Silver oxide (0.024 g, 0.10 mmol) was added to a solution of ${\bf 1a}$ or ${\bf 1b}$ (0.20 mmol) on dichloromethane. The mixture was protected from light and stirred for 4 h at room temperature. Then the solution was filtered through Celite and the solution was reduced to minimum volume under vacuum. A grey oily solid was obtained and washed with diethyl ether.

[AgI(IPyOct)] (4a). Yield: 96 %. 1 H RMN (400 MHz, CDCl₃, δ (ppm)): 8.54–8.46 (m, 1H, Py), 8.15 (d, $J_{H-H}=8.2$, 2H, Py), 7.92–7.85 (m, 1H, Py), 7.82 (d, $J_{H-H}=2$, 1H, Im), 7.40–7.37 (m, 1H, Py), 7.13 (d, $J_{H-H}=2$ Hz, 1H, Im), 4.26 (t, $J_{H-H}=7.2$ Hz, 2H, CH_2-N), 1.95–1.80 (m, 2H, CH_2-CH_2-N), 1.44–1.17 (m, 10H, $-CH_2-$), 0.88 (t, $J_{H-H}=6.8$, 3H, CH_3) 13 C 1 H}-APT RMN (75 MHz, CDCl₃, δ (ppm)): 191.4 (Im_{carb}), 149.0 (Py), 139.3 (Py), 123.7 (Py), 121.3 (Im), 119.9 (Im), 115.2 (Py), 52.9 (CH₂), 31.7 (CH₂), 31.4 (CH₂), 29.1 (CH₂), 29.1 (CH₂), 26.5 (CH₂), 22.6 (CH₂), 14.1 (CH₃). MS (MALDI⁺): m/z (%) = 621.3 (100 %) [(IOctPy)₂Ag]⁺, m/z (%) = 364.2 (25.36 %) [M-I]⁺, m/z (%) = 258.1 (100 %) [M-AgI]⁺. HRMS (ESI-QTOF) m/z: [M-I]⁺ calcd for $C_{16}H_{23}AgN_3$, Exact Mass: 364.0942; found, 365.0895 and [(IOctPy)₂Ag]⁺ calcd for $C_{32}H_{46}AgN_6$, Exact Mass: 621.2834; found, 621.2810.

[AgI(IBnOct)] (4b). Yield: 76 %. 1 H RMN (400 MHz, CDCl₃, δ (ppm),): 7.36–7.30 (m, 3H, Ph), 7.27–7.23 (m, 2H, Ph), 6.95 (d, J_{H-H} = 1.8 Hz, 1H, Py), 6.88 (d, J_{H-H} = 1.8 Hz, 1H, Py), 5.32 (s, 2H, N- CH_2 -Ph), 4.13 (t, J = 7.5 Hz, 2H, CH₂-N), 1.90–1.70 (m, 2H, CH_2 -CH₂-N), 1.40–1.15 (m, 10H, -CH₂-), 0.87 (t, J_{H-H} = 6.8 Hz, 3H, CH₃). 13 C{ 1 H}-APT RMN (75 MHz, CDCl₃, δ (ppm)): 129.1 (Ph), 128.7 (Ph), 127.9 (Ph), 121.1 (Im), 120.8 (Im), 55.7 (CH₂), 52.1 (CH_2 -Ph), 31.7 (CH₂), 31.4 (CH₂), 29.1 (CH₂), 29.1 (CH₂), 26.5 (CH₂), 22.6 (CH₂), 14.1 (CH₃). MS (MALDI⁺): m/z (%) = 647.4 (99.47 %) [(IBnOct)₂Ag]⁺, m/z (%) = 377.2 (10.79 %) [M-I]⁺, m/z (%) = 271.1 (100 %) [M-AgI]⁺. HRMS (ESI-QTOF) m/z: [(IOctBn)₂Ag]⁺ calcd for C₃₆H₅₂AgN₄, Exact Mass: 647.3243; found, 647.3386.

4.4. Synthesis of gold derivatives

4.4.1. Synthesis of [AuCl(IROct)]

[AuCl(tht)] (0.12 mmol) was added to a solution of 4a or 4b (0.12 mmol) in dichloromethane (15 mL). The mixture was protected from light and stirred for 4 h at room temperature. The white AgCl precipitate obtained was filtered through Celite and the solution was reduced to dryness under vacuum. An orange oil was isolated.

[AuCl(IPyOct)] (5a). Yield: 95 %. 1 H RMN (400 MHz. CDCl₃. δ (ppm)): 8.68–8.62 (m. 1H, Py). 8.54–8.49 (m, 1H, Py), 8.99–7.90 (m, 1H, Py), 7.96–7.83 (m, 1H, Py), 7.82 (d, $J_{H-H}=2.1$ Hz, 1H, Im), 7.43–7.36 (m, 1H, Py), 7.10 (d, $J_{H-H}=2.1$ Hz, 1H, Im), 4.32 (t, $J_{H-H}=7.2$ Hz, 2H, CH_2 -N), 2.14–1.86 (m, 2H, CH_2 -CH₂-N), 1.47–1.17 (m, 10H, CH_2 -), 0.88 (t, $J_{H-H}=6.9$, 3H, CH_3). 13 C(1 H}-APT RMN (75 MHz, CDCl₃. δ (ppm)): 148.8 (Py), 139.1 (Py), 123.9 (Py), 121.6 (Im), 120.7 (Im), 117.4 (Py), 52.6 (CH₂), 31.7 (CH₂), 31.0 (CH₂), 29.1 (CH₂), 29.0 (CH₂), 26.5 (CH₂), 22.6 (CH₂), 14.1 (CH₃). MS (MALDI⁺): m/z (%) = 711.13 (100 %) [(IPyOct)₂Au]⁺. HRMS (ESI-QTOF) m/z: [(IPyOct)₂Au]⁺ calcd for C_{32} H₄₆AuN₆, Exact Mass: 711.3449; found, 711.3468.

[AuCl(IBnOct)] (**5b**). Yield: 87 %. 1 H RMN (400 MHz, CDCl₃, δ (ppm)): 7.40–7.28 (m, 5H, Ph), 6.92 (d, $J_{H-H}=2.1$ Hz, 1H, Im), 6.86 (d, $J_{H-H}=2.1$ Hz, 1H, Im), 5.37 (s, 2H, N- CH_2 -Ph), 4.18 (t, $J_{H-H}=7.5$ Hz, 2H, CH_2 -N), 1.92–1.79 (m, 2H, CH_2 -CH₂-N), 1.40–1.18 (m, 10H, -CH₂-), 0.87 (t, $J_{H-H}=7.5$ Hz, 3H, CH₃). 13 C(1 H}-APT RMN (75 MHz, CDCl₃, δ (ppm)): 135.5 (Ph), 129.1 (Ph), 128.7 (Ph), 120.8 (Im), 120.1 (Im), 55.2 (CH_2 -Ph), 51.6 (CH₂), 31.7 (CH₂), 31.05 (CH₂), 29.1 (CH₂), 26.4 (CH₂), 22.6 (CH₂), 14.05 (CH₃). MS (MALDI⁺): m/z (%) = 737.4 (98.59 %) [(IBnOct)₂Au]⁺, m/z (%) = 159.0 (27.90 %) [IBn]⁺. HRMS (ESI-QTOF) m/z: [(IBnOct)₂Au]⁺ calcd for C₃₆H₅₂AuN₄, Exact Mass: 737.3857; found, 737.3915 and [M + Na]⁺ calcd for C₁₈H₂₆AuClN₂Na, Exact Mass: 525.1347; found, 525.1342. Anal. Calcd (%) for C₁₈H₂₇AuClN₂

(502.83): C, 43.00; H, 5.21; N, 5.57. Found: C, 42.71; H, 5.18; N, 5.8.

4.4.2. Synthesis of [AuCl(IRR_f)] ($R_f = OctF = -(CH_2)_2C_6F_{13}$)

 $NBu_4(acac)$ (0.15 mmol) was added to a solution of [AuCl(tht)] (0.15 mmol) and ${\bf 3a}$ or ${\bf 3b}$ (0.15 mmol) in dichloromethane (15 mL). The mixture was reacted at room temperature for 24 h. The solution was reduced to dryness under vacuum and the crude was then eluted with dichloromethane on silica gel to afford white solid.

[AuCl(IPyOctF)] (**6a**). Yield: 60 %. 1 H RMN (400 MHz, CDCl₃, 8 (ppm)): 8.59 (d, $J_{HH} = 8.1$ Hz, 1H, Py), 8.53 (d, $J_{HH} = 3.7$ Hz, 1H, Py), 7.94 (td, $J_{HH} = 8.1$ Hz, 1.7, 1H, Py), 7.85 (d, $J_{HH} = 2$ Hz, 1H, Im), 7.43 (dd, $J_{HH} = 7.2$ Hz, 5.1, 1H, Py), 7.22 (d, $J_{HH} = 2$ Hz, 1H, Im), 4.64 (t. $J_{HH} = 6.8$ Hz, 2H, CH_{2} -N), 2.91–2.78 (m, 2H, CH_{2} -CH₂-N). 13 C{ 1 H}-APT RMN (75 MHz, CDCl₃, 8 (ppm)): 182.1 (Im_{carb}), 150.5 (Py), 148.9 (Py), 139.2 (Py), 124.4 (Py), 121.5 (Im), 120.9–110.0 (m series, 6C, -CH₂-CF₂-CF₂-, -CH₂-CF₂-CF₂-, -CH₂-(CF₂)₂-CF₂-, -CH₂-(CF₂)₃-CF₂-, -CH₂-(CF₂)₄-CF₂-CF₃), 120.8 (Im), 117.3 (Py), 44.5 (CH_{2} -R_f), 32.3 (m, CH₂-CH₂-R_f). 19 F{ 1 H} RMN (377 MHz, CDCl₃, 8 (ppm)): $^{-80.75}$ (t, $J_{FF} = 9.9$ Hz, 3F, CF₃), $^{-1}$ 13.27 (m, 2F, CF₂), $^{-1}$ 21.72 (m, 2F, CF₂), $^{-1}$ 22.77 (s, 2F, CF₂), $^{-1}$ 23.15 (m, 2F, CF₂), $^{-1}$ 26.09 (m, 2F, CF₂). MS (MALDI+): m/z (%) $^{-1}$ 20.505 (10 %) [M-Cl]+, 1179 (75 %) [(IPyR_f)₂Au]+. Anal. Calcd (%) for C₁₆H₁₀AuClF₁₃N₃ (723.67): C, 26.56; H, 1.39; N, 5.81. Found: C, 26.87; H, 1.45; N, 5.55.

[AuCl(IBnOctF)] (6b). Yield: 87 %. 1 H RMN (300 MHz, CDCl₃, δ (ppm)): 7.41–7.27 (m, 5H, Ph), 7.10–6.99 (m, 1H, Im), 6.92–6.88 (m, 1H, Im), 5.39 (s, 2H, N-CH₂-Ph), 4.51 (t. $J_{H-H} = 7.5$ Hz, 2H, CH_2 -N), 2.87–2.65 (m, 2H, CH_2 -CH₂-N). 13 C{ 1 H}-APT RMN (75 MHz. CDCl₃, δ (ppm)): 184.1 (Im_{carb}), 135.1 (Ph), 129.4 (Ph), 129.1 (Ph), 128.7 (Ph), 1128.0 (Ph), 127.2 (Ph), 122.4 (Im), 122.3 (Im), 120.7–110.4 (m series, 6C, -CH₂-CF₂-CF₂-, -CH₂-CF₂-CF₂-, -CH₂-(CF₂)₃-CF₂-, -CH₂-(CF₂)₄-CF₂-CF₃), 54.9 (CH_2 Ph), 43.6 (CH_2 -R_f), 31.8 (m, CH₂-CH₂-R_f). 19 F{ 1 H} RMN (282 MHz, CDCl₃, δ (ppm)): -80.75 (tt, $J_{F-F} = 9.9$ Hz, 2.3, 3F, CF₃), -113.44 (m, 2F, CF₂), -121.77 (m, 2F, CF₂), -122.81 (s, 2F, CF₂), -123.23 (m, 2F, CF₂), -126.09 (m, 2F, CF₂). MS (MALDI⁺): m/z (%) = 1205.2 (8.02 %) [(IBnR_f)₂Au]⁺. Anal. Calcd (%) for C₁₈H₁₃AuClF₁₃N₂ (736.71): C, 29.35; H, 1.78; N, 3.80. Found: C, 29.47; H, 2.15; N, 3.55.

4.4.3. Synthesis of [Au(Spy)(IROct)]

[AuCl(IROct)] (0.12 mmol) was added to a solution of 2-mercapto pyridine (0.12 mmol) in dichloromethane (15 mL) with $\rm Cs_2CO_3$ (1.75 mmol). The mixture was stirred for 4 h at room temperature. The solution was filtered through Celite and the solution was reduced to dryness under vacuum. A yellow oil was isolated.

[Au(SPy)(IPyOct)]. (7a). Yield: 98 %. 1 H RMN (400 MHz, CDCl₃, δ (ppm), J (Hz)): 9.07–8.94 (m, 1H, Py), 8.28–8.17 (m, 1H, SPy), 7.90 (d, $J_{H:H} = 1.8$, 1H, Im), 7.88–7.79 (m, 1H, Py), 7.65–7.59 (m, 1H, SPy), 7.55–7.45 (m, 1H, Py), 7.39–7.32 (m, 1H, Py), 7.15–7.09 (m, 1H, Spy), 7.09 (d, $J_{H:H} = 1.8$, 1H, Im), 6.81 (ddd, $J_{H:H} = 7.2$; 5.1; 1, 1H, SPy), 4.38 (t, $J_{H:H} = 7.5$, 2H, CH₂-N), 2.02–1.88 (m, 2H, CH₂-CH₂-N), 1.47–1.15 (m, 10H, -C₅H₁₀-), 0.86 (m, $J_{H:H} = 6.9$, 3H, CH₃). 13 C{ 1 H}-APT RMN (75 MHz, CDCl₃, δ (ppm)): 149.6 (Py); 148.5 (Py); 139.0 (Py); 137.4 (Py); 123.5 (Py); 121.1 (Im); 120.6 (Im); 119.7 (Py); 117.7 (Py); 117.3 (Py); 52.4 (CH₂); 31.7 (CH₂); 31.1 (CH₂); 29.1 (CH₂); 26.5 (CH₂); 22.6 (CH₂); 14.05 (CH₃) MS (MALDI+): m/z (%) = 711.4 (100 %) [(IPyOct)₂Au]⁺. Anal. Calcd (%) for C₂₁H₂₇AuN₄S (564.50): C, 44.68; H, 4.82; N, 9.93; S, 5.68. Found: C, 44.32; H, 4.41; N, 9.68; S, 5.42.

[Au(SPy)(IBnOct)]. (**7b**). Yield: 91 %. 1 H RMN (300 MHz, CDCl₃, δ (ppm), J (Hz)): 8.26–8.14 (m, 1H, SPy), 7.68–7.49 (m, 1H, SPy), 7.43–7.28 (m, 5H, Ph), 7.25–7.18 (m, 1H, SPy), 6.91 (d, $J_{H-H} = 1.8$, 1H, Im), 6.86 (d, $J_{H-H} = 1.8$, 1H, Im), 6.82–6.74 (m, 1H, SPy), 5.44 (s, 2H, N-CH₂-Ph), 4.23 (t, $J_{H-H} = 7.5$, 2H, CH₂-N), 1.96–1.81 (m, 2H, CH₂-CH₂-N), 1.41–1.20 (m, 10H, -C₅H₁₀-), 0.86 (t, $J_{H-H} = 7.2$, 3H, CH₃) 13 C(1 H}-APT RMN (75 MHz, CDCl₃, δ (ppm)): 148.5 (Py); 134.9 (Py); 129.0 (Ph); 128,56 (Ph); 128.2 (Ph); 127.4 (Py); 120.7 (Im); 119.7 (Im); 117.6 (Py); 54.9 (CH₂-Ph); 51.4 (CH₂); 31.7 (CH₂); 31.1 (CH₂); 29.1 (CH₂); 26.5

(CH₂); 22.6 (CH₂); 14.05 (CH₃) MS (MALDI⁺): m/z (%) = 737.4 (100 %) [(IBnOct)₂Au]⁺. Anal. Calcd (%) for $C_{23}H_{30}AuN_3S$ (577.54): C, 47.83; H, 5.24; N, 7.28; S, 5.55. Found: C, 48.12; H, 7.33; N, 6.02; S, 5.90. HRMS (ESI-QTOF) m/z: M^+ calcd for $C_{23}H_{30}AuN_3S$, Exact Mass: 577.1826; found, 578.1895.

[Au(SPy)(IPyOctF)]. (8a). Yield: 66 %. 1 H RMN (400 MHz, CDCl₃, δ (ppm), J (Hz)): 8.9 (d, $J_{H:H}$ = 7.7, 1H, Py), 8.44 (d, $J_{H:H}$ = 3.9, 1H, SPy), 8.15–8.10 (m, Py), 7.86–7.80 (m, 2H, Im + Py), 7.50–7.42 (m, 1H, SPy), 7.37–7.28 (m, 1H, Py), 7.23–7.17 (m, 1H, SPy), 7.08 (s, 1H, Im), 6.77–6.75 (m, 1H, SPy), 4.66 (t, $J_{H:H}$ = 6.7, 2H, CH₂-N), 2.91–2.81 (m, 2H, CH₂-CH₂-N). 13 C{ 1 H}-APT RMN (75 MHz, CDCl₃, δ (ppm)): 167.0 (Im_{carb}), 150.2 (Py); 149.6 (Py); 139.1 (Py); 124.0 (Py); 121.4 (Im); 120.4 (Im); 120–110.1 (m series, 6C, -CH₂-CF₂-CF₂-, -CH₂-CF₂-CF₂-CF₂-C-CH₂-(CF₂)₃-CF₂-, -CH₂-(CF₂)₄-CF₂-CF₃), 117.8 (Py); 117.3 (Py); 44.4 (CH₂-Rf), 32.5 (m, CH₂-CH₂-Rf). 19 F{ 1 H}RMN (377 MHz, CDCl₃, δ (ppm), J (Hz)): −80,68 (m, 3F, CF₃), −113,22 (m, 2F, CF₂), −121,73 (m, 2F, CF₂), −122,74 (s, 2F, CF₂), −123,05 (m, 2F, CF₂), −126,01 (m, 2F, CF₂). MS (MALDI⁺): m/z (%) = 1181.5 (92 %) [(IPyOctF)₂Au]⁺. Anal. Calcd (%) for C₂₁H₁₄AuF₁₃N₄S (798.37): C, 31.59; H, 1.77; N, 7.02; S, 4.02. Found: C, 31.23; H, 1.57; N, 6.84; S, 4.11.

[Au(SPy)(IBnOctF)]. (**8b**). Yield: 96 %. ¹H RMN (400 MHz, CDCl₃, δ (ppm), J (Hz)): 8.17 (ddd, J_{H-H} = 4.9; 1.8; 0.8, 1H, SPy), 7.47 (dt, J_{H-H} = 8; 1, 1H, SPy), 7.42-7.32 (m, 5H, Ph), 7.28-7.24 (m, 1H, SPy), 6.98 (d, $J_{H-H} = 2$, 1H, Im), 6.9 (d, $J_{H-H} = 2$, 1H, Im), 6.79 (ddd, $J_{H-H} = 7.3$; 5; 1.1, 1H, SPy), 5.46 (s, 2H, N- CH_2 -Ph), 4.57 (t, $J_{H-H} = 6.9$, 2H, CH_2 -N), 2.96-2.78 (m, 2H, CH₂-CH₂-N). ¹³C{¹H}-APT RMN (75 MHz, CDCl₃, δ (ppm)): 167.4 (Im_{carb}), 148.1 (Ph), 135.3 (Ph), 134.9 (Ph), 129.1 (Ph), 128.8 (Ph), 128.2 (Ph), 126.9 (Ph), 121.5 (Im), 121-110.0 (m series, 6C, -CH₂-CF₂-CF₂-, -CH₂-CF₂-CF₂-, -CH₂-(CF₂)₂-CF₂-, -CH₂-(CF₂)₃-CF₂-, -CH₂-(CF₂)₄-CF₂-CF₃), 120.4 (Im), 117.8 (Py), 117.6 (Py), 55.3 (CH₂Ph), 43.5 (CH₂-Rf), 32.6 (m, CH₂-CH₂-Rf), ¹⁹F{¹H}RMN (377 MHz, CDCl₃, δ (ppm), J (Hz)): -80,70 (tt, $J_{F-F} = 9,8$, $J_{F-F} = 2,2$, 3F, CF_3), -113,51 (m, 2F, CF₂), -121,8 (m, 2F, CF₂), -122,8 (s, 2F, CF₂), -123,2 (m, 2F, CF₂), -126,1 (m, 2F, CF₂). MS (MALDI⁺): m/z (%) = 1205,1 (95,48 %) [(IBnOctF)₂Au]⁺. Anal. Calcd (%) for C₂₃H₁₇AuF₁₃N₃S (811.45): C, 34.05; H, 2.11; N, 5.18; S, 3.95. Found: C, 34.04; H, 1.72; N, 5.19; S, 3.98. HRMS (ESI-QTOF) $\emph{m/z}$: $[M + H]^+$ calcd for $C_{23}H_{18}AuF_{13}N_3S$, Exact Mass: 812.0691; found, 812.0677.

4.4.4. Synthesis of $[Au(IRR')_2]X$ (R = Py. Bn; $X = BF_4$; R' = Oct; X = TfO. $R' = -(CH_2)_2C_6F_{13}$)

[AuCl(tht)] (0.1 mmol) was added to a solution of 9a or 9b or 3a or 3b (0.1 mmol) and Cs_2CO_3 (1.4 mmol) in dichloromethane (15 mL). The mixture was stirred for 24 h at room temperature. The solution obtained was filtered through Celite and the reduced to minimum volume under vacuum and precipitated with diethyl ether. A pale yellow solid was obtained and washed with diethyl ether.

[Au(IOctPy)₂]BF₄ (**10a**). Yield: 63 %. 1 H RMN (400 MHz. CDCl₃. δ (ppm)): 9.46–8.45 (m. 1H. Py). 8.13–8.11 (m. 1H. Py). 7.89–7.85 (m. 1H. Py). 7.72 (d. $J_{H:H}=2$ Hz. 1H. Im). 7.44–7.41 (m. 1H. Py). 7.40 (d. $J_{H:H}=2$ Hz. 1H. Im). 4.31 (t. $J_{H:H}=7.2$ Hz. 2H. CH_2 -N). 1.93–1.87 (m. 2H. CH_2 -CH₂-N). 1.22–1.18 (m. 10H. -CH₂-). 0.84 (t. $J_{H:H}=6.9$ Hz. 3H. CH₃). 19 F{ 1 H} RMN (377 MHz. CDCl₃. δ (ppm)): -148.24. 13 C(1 H}-APT RMN (75.5 MHz. CDCl₃. δ (ppm)): 181.2(s. Im_{carb}), 150.5 (Py), 148.9 (Py), 139.4 (Py), 124.2 (Py), 117.3 (Py), 122.4 (Im), 121.2 (Im), 52.4 (CH₂). 31.7 (CH₂), 31.3 (CH₂), 29.2 (CH₂), 29.1 (CH₂), 26.5 (CH₂), 22.6 (CH₂), 14.0 (CH₃). MS (MALDI⁺): m/z (%) = 711.4 (100 %) [M]⁺. Anal. Calcd (%) for C₃₂H₄₆AuBF₄N₆ (798.53): C, 48.13; H, 5.81; N, 10.52. Found: C, 47.86; H, 5.65; N, 10.22.

[Au(IBnOct)₂]BF₄ (**10b**). Yield: 73 %. 1 H RMN (400 MHz. CDCl₃. δ (ppm)): 7.34–7.17 (m. 1H. Ph). 7.16 and 7.15 (AB system. $J_{H-H}=2$ Hz. 2H. Im). 5.31 (s. 2H. N- CH_2 -Ph). 4.14 (t. $J_{H-H}=7.1$ Hz. 2H. CH_2 -N). 1.85–1.82 (m. 2H. CH_2 -CH₂-N). 1.26–1.19 (m. 10H. -CH₂-). 0.86 (t. $J_{H-H}=7.2$ Hz. 3H. CH₃). 19 F{ 1 H} RMN (377 MHz. CDCl₃. δ (ppm)): -148.24. 13 C{ 1 H}-APT RMN (75.5 MHz. CDCl₃. δ (ppm)): 183.4 (s. Im_{carb}), 135.7

(Ph), 129.0 (Ph), 128.5 (Ph), 127.3 (Ph), 122.3 (Im), 122.0 (Im), 54.7 (CH_2 -Ph), 51.5 (CH_2), 31.7 (CH_2), 31.5 (CH_2), 29.2 (CH_2), 29.1 (CH_2), 26.5 (CH_2), 22.6 (CH_2), 14.05 (CH_3). MS (MALDI⁺): m/z (%) = 737.4 (100 %) [M]⁺. HRMS (ESI-QTOF) m/z: M⁺ calcd for $C_{36}H_{52}AuN_4$, Exact Mass: 737.3857; found, 737.3867. Anal. Calcd (%) for $C_{36}H_{52}AuBF_4N_4$ (824.61): $C_{36}H_{52}AuBF_4N_4$

[Au(IPyOctF)₂]TfO (OctF = $-(CH_2)_2C_6F_{13}$) (11a). Yield: 63 %, 1H RMN (400 MHz, CDCl₃, δ (ppm)): 8.42–8.41 (m, 1H, Py), 8.07–8.06 (m, 1H, Py), 7.80–7.78 (m, 2H, Py + Im), 7.51 (d, $J_{H-H} = 2$ Hz, 1H, Im), 7.38 (ddd, $J_{H-H} = 7.5$ Hz, 4.9; 0.8, 1H, Py), 4.74 (t, $J_{H-H} = 6.9$ Hz, 2H, CH_2 -N), 2.87–2.75 (m, 2H, CH_2 -CH₂-N). $^{13}C_4^{11}H_3$ -APT RMN (75.5 MHz, CDCl₃. δ (ppm)): 181.9 (Im_{carb}), 150.3 (Py), 148.9 (Py), 139.4 (Py), 124.4 (Py), 122.5 (Im), 121.6 (Im), 120.2–108.0 (m series, 6C, -CH₂-CF₂-CF₂-, -CH₂-CF₂-CF₂-, -CH₂-(CF₂)₃-CF₂-, -CH₂-(CF₂)₃-CF₂-, -CH₂-(CF₂)₄-CF₂-CF₃), 117.5 (Py), 44.4 (CH_2 -R_f), 32.1 (m, CH_2 - CH_2 -R_f). $^{19}F_4^{1}H_3$ RMN (377 MHz, CDCl₃, δ (ppm)): $^{-7}8.47$ (s, TfO), $^{-8}0.92$ (t, $^{-1}2.49$ H, RMN (373, $^{-1}2.49$ (s, 2F, CF₂), $^{-1}2.49$ (m, 2F, CF₂), $^{-1}2.49$ (s, 2F, CF₂), $^{-1}2.49$ (s, 2F, CF₂), $^{-1}2.49$ (s) [M] $^{+}$. Anal. Calcd (%) for $C_{33}H_{20}AuF_{29}N_6O_3S$ (1328.54): C, 29.83; H, 1.52; N, 6.33; S, 2.41. Found: C, 29.52; H, 1.35; N, 6.22; S, 2.20.

[Au(IBnOctF)₂]TfO (OctF = $-(CH_2)_2C_6F_{13}$) (11b). Yield: 70 %, 1H RMN (400 MHz, CDCl₃, δ (ppm)): 7.36–7.28 (m, 4H, pH + Im), 7.14–7.12 (m, 2H, Ph), 7.06 (d, $J_{H\cdot H} = 1.8$ Hz, 1H, Im), 5.25 (s, 1H, CH₂Ph), 4.58 (t, $J_{H\cdot H} = 6.7$ Hz, 2H, CH_2 -N), 2.78–2.66 (m, 2H, CH_2 -CH₂-N). 13 C{ 1H }-APT RMN (75.5 MHz, CDCl₃, δ (ppm)): 184.0 (Im_{carb}), 135.2 (Ph). 129.1 (Ph), 128.7 (Ph), 127.2 (Ph), 122.5 (Im), 122.3 (Im), 120.3–107.7 (m series, 6C, $^-CH_2$ - $^-CF_2$ - $^$

4.5. Stability in buffered solution and distribution coefficient (logP)

The stability of the gold complexes has been analysed by absorption UV–vis spectroscopy. The absorption spectra of the complexes were recorded on a Thermo Scientific spectrophotometer.

Solutions of these complexes (5 \times 10⁻⁵ M) in PBS (pH = 7.4) were prepared from 10 mM DMSO stock solutions of the complexes and thereafter monitored measuring the electronic spectra over 24 h under incubation at 37 °C.

The n-octanol-water coefficients of the complexes were determined by using a shake-flask method. Buffered-saline distilled water (100 mL, phosphate buffer $[PO_4^{3-}] = 10$ mM, [NaCl] = 0.15 M, pH 7.4) and n-octanol (100 mL) were shaken for 72 h to allow saturation of both phases. 1 mg of the new complexes was dissolved in 4 mL of the aqueous phase and 4 mL of the organic phase were added, mixing for 10 min. The resulting emulsion was centrifuged to separate the phases. The concentration of the compounds in each phase was determined using UV absorbance spectroscopy. LogP was defined as log{[compound (organic)]/[compound(aqueous)]}.

4.6. Cell culture, cell treatment and determination of cell viability

The human Caco-2 cell line (clone TC7) was kindly provided by Dr. Edith Brot-Laroche (Université Pierre et Marie Curie-Paris 6, UMR S 872, Les Cordeliers, France). The mouse liver cell line (AML12) was provided by ATCC collection (Manassas, VA, USA). The cell lines were maintained in a humidified atmosphere with 5 % CO2 at 37 °C. Caco-2 cells were cultured in Dulbecco's modified Eagle's medium (DMEM) (Gibco Invitrogen, Paisley, UK) supplemented with 20 % fetal bovine serum (FBS),

 $1\ \%$ nonessential amino acids, $1\ \%$ penicillin (1000 U/mL), $1\ \%$ streptomycin (1000 µg/mL), and $1\ \%$ amphotericin (250 U/mL). AML12 cells were cultured in DMEM (Thermo Fisher Scientific, Waltham, MA, USA): F-12-Ham's medium (GE Healthcare Life Science, South Logan, UT, USA) at a 1:1 ratio supplemented with $10\ \%$ fetal bovine serum (Thermo Fisher Scientific, Waltham, MA, USA), $1:\ 500$ insulin—transferrin—selenium (Corning, Bedford, MA, USA), $40\ ng/mL$ dexamethasone (Sigma-Aldrich; Merck Millipore, Darmstadt, Germany), $1\ \%$ non-essential amino acids (Thermo Fisher Scientific, Waltham, MA, USA), $1\ \%$ amphotericin B (1000 mg/mL; Thermo Fisher Scientific, Waltham, MA, USA), $1\ \%$ penicillin (1000 U/mL; Thermo Fisher Scientific, Waltham, MA, USA), and $1\ \%$ streptomycin (1000 mg/mL; Thermo Fisher Scientific, Waltham, MA, USA).

Cells were enzymatically treated with 0.25 % trypsin-1 mM EDTA and subcultured into 25 cm² plastic flasks at a density of 5×10^5 cells/ cm². The culture medium was replaced every 2 days. Metal complex treatments were added 24 h after seeding to have undifferentiated Caco-2 cells, [56] The complexes were diluted in cell culture medium to a final concentration of 20 mM. For cytotoxicity detection assays, cells were seeded into 96-well plates at a density of 4×10^3 cells/well. The culture medium was replaced with medium containing metal complexes or DMSO (used as a control) and the cells were incubated for 72 h. The antiproliferative effect was measured using the 3-(4,5-dimethyl-2-thiazoyl)-2,5-diphenyltetrazolium bromide (MTT) assay, as previously described.[49] After 72 h of incubation with the complexes, 10 µL of MTT (5 mg/mL) was added and incubation was continued at 37 $^{\circ}$ C for 3 h. The medium was removed by inversion and 100 μL of DMSO was added to each well. The absorbance at 560 nm, proportional to many living cells, was measured by spectrophotometry (SPECTROstar Nano, BMG LABTECH) and converted to a percentage (%) of growth inhibition. The effect on cell growth was expressed as a percentage of the control. Finally, the IC₅₀ value at 72 h was calculated. This value represents the concentration of the compound that reduces cell proliferation or viability by half.

Metal complex treatments were added 24 h after plating for assays on differentiated Caco-2 cells, which had been cultured on 96-well plates under standard culture conditions for 15 days., Cell confluence (80 %) until reaching 80 % confluence confirmed by observation under an optical microscope.

4.7. Evaluation of cell apoptosis

After the appropriate incubation, cells were collected and stained with Annexin V-FTIC according to the manufacturer's instructions. A negative control was prepared containing unreacted cells to define the basal level of apoptotic and necrotic or dead cells. After incubation, cells were transferred to flow-cytometry tubes and washed twice with temperate phosphate-buffered saline (PBS), suspended in 100 μL annexin V binding buffer (10 mM Hepes/NaOH, pH 7.4, 140 mM NaCl, 2.5 mM CaCl₂), then 5 μL of annexin V-FITC and 5 μL of PI was to each 100 μL of cell suspension. After incubation for 15 min at room temperature in the dark, 400 μL of $1\times$ annexin binding buffer was added and analysed by flow cytometry within one hour. The signal intensity was measured using a FACSARIA BD and analysed using FASCDIVA BD.

4.8. Determination of mitochondrial membrane potential and activity of caspase 3

To determine mitochondrial potential and caspase-3 activity, cells were seeded in 25 cm² flasks and then exposed to gold compounds for 24 h. Control cells were incubated with a medium without compounds. Then, the method previously described by our research group was followed [57].

4.9. Analysis of cell cycle and DNA content

After treatment, the cells were fixed in 70 % ice-cold ethanol and stored at 4 °C for 24 h. After centrifugation, the cells were rehydrated in PBS (phosphate buffered saline) and stained with propidium iodide (PI, 50 $\mu g/mL)$ solution containing RNase A (100 $\mu g/mL)$. PI-stained cells were analysed for DNA content in a FACSARRAY BD equipped with an argon ion laser. The red fluorescence emitted by PI was collected using a 620 nm longer pass filter as a measure of the amount of DNA-bound PI and displayed on a linear scale. Cell cycle distribution was determined on a linear scale. The percentage of cells in cycle phases was determined using MODIFIT 3.0 verity software.

4.10. Intracellular levels of reactive oxygen species (ROS) determination

Caco-2 cells were seeded in a 96-well plate at a density of 4×10^3 cells/well. Intracellular ROS levels were determined using the dichlor-ofluorescein assay [25]. The IC $_{50}$ concentration of the selected compounds was added for an additional 24 h. One group of cells was incubated with the complexes at 37 °C, while in another group, the cells were incubated with the gold compounds for 1 h at 41 °C and then for 23 h at 37 °C. Thereafter, the cells were incubated with 20 μ M 2′,7′-dichlorofluorescein diacetate (DCFH-DA) (Merck KGaA, Darmstadt, Germany) in DMEM. The generation of oxidized derivative DCF was monitored by measuring the increase of fluorescence for 1 h, at an emission wavelength of 520 nm and excitation of 485 nm, with a FLUOstar Omega (BMG Labtech, Ortenberg, Germany) multiplate reader. The results were expressed as a percentage of fluorescence relative to the control, with the understanding that the fluorescence intensity reflected the intracellular ROS levels.

4.11. Intracellular TrxR activity

The method is based on the reaction of 2,2'-dinitro-5,5'-dithiobenzoic acid (DTNB) with thiol groups of proteins to form the 2-nitro-5-thiobenzoate anion (TNB2-), which absorbs at $\lambda_{\text{max}} = 412 \text{ nm.}$ Caco-2 cells were seeded in a 25 cm² flask (2 \times 10⁶). After 24 h, the IC₅₀ concentration of the selected compounds was added for 24 h. One group of cells was incubated with the complexes at 37 $^{\circ}\text{C}$ and in another group, the cells were incubated with the metallic compounds for 2 h at 41 °C and then for 22 h at 37 °C. All cells were then harvested and lysed using the M-PER® mammalian protein extraction reagent (commercial reference Thermo Fisher Scientific, 78501) following the supplier's instructions. The interaction of metal complexes with the enzyme thioredoxin reductase was analysed using a thioredoxin reductase assay kit (Sigma, CS0170, St Louis, MO, USA). The procedural guidelines of the supplied kit were followed. The reaction was started with the introduction of DTNB (100 mM) and the transformation to TNB was observed at 412 nm at 30 s intervals for 5 min, using a SPECTRO-star Nano multiplate reader from BMG Labtech. Results were presented as a percentage representing TrxR activity relative to control. The activity of untreated cells was considered the control and estimated as 100 % of the activity.

4.12. Statistical analyses

Results are presented as mean \pm SD. One-way analysis of variance was used to compare means (ANOVA). We used the Bonferroni multiple comparison test to compare differences that were statistically significant at p < 0.05. GraphPad software, San Diego, CA, USA (GraphPad Prism version 5.02) was used for statistical analysis and graphical.

CRediT authorship contribution statement

Javier Quero: Investigation, Formal analysis, Data curation. Adrián Alconchel: Investigation, Formal analysis, Data curation. Sara Ortega: Investigation. Seyed Hesamoddin Bidooki: Investigation, Formal

analysis, Data curation. Ma. Concepción Gimeno: Writing – review & editing, Funding acquisition. Ma. Jesús Rodriguez-Yoldi: Writing – review & editing, Supervision, Investigation, Funding acquisition, Data curation, Conceptualization. Elena Cerrada: Writing – review & editing, Writing – original draft, Supervision, Investigation, Funding acquisition, Conceptualization.

Declaration of competing interest

The authors declare the following financial interests/personal relationships which may be considered as potential competing interests (Elena Cerrada reports financial support was provided by University of Zaragoza. Elena Cerrada reports a relationship with University of Zaragoza that includes: employment. If there are other authors, they declare that they have no known competing financial interests or personal relationships that could have appeared to influence the work reported in this paper.)

Acknowledgments

The authors thank project PID2022-136861NB-I00 funded by MICIU/AEI10.13039/501100011033, the Ministerio de Ciencia e Innovación-Fondo Europeo de Desarrollo Regional (PID2022-136414OB-I00), Interreg Sudoe Program (NEWPOWER, S1/1.1/E01116) and CIBER Fisiopatología de la Obesidad y la Nutrición as an initiative of FEDER-ICCIII (CIBEROBN, CB06/03/1012) and Gobierno de Aragón (Research Groups E07_23R and B16_23R). Seyed Hesamoddin Bidooki is funded through a research contract with the University of Zaragoza, within the framework of the Sudoe-NEWPOWER Project (S1/1.1/E01116). Authors thank to Centro de Investigación Biomédica de Aragón (CIBA), España for technical assistance: http://www.iacs.aragon.es, use of Servicio General de Apoyo a la Investigación-SAI, Universidad de Zaragoza.

Appendix A. Supplementary data

Supplementary data to this article can be found online at https://doi.org/10.1016/j.jinorgbio.2025.112987.

Data availability

The data that has been used is confidential.

References

- [1] L. Botta, L. Dal Maso, S. Guzzinati, C. Panato, G. Gatta, A. Trama, M. Rugge, G. Tagliabue, C. Casella, B. Caruso, M. Michiara, S. Ferretti, F. Sensi, R. Tumino, F. Toffolutti, A.G. Russo, A.L. Caiazzo, L. Mangone, W. Mazzucco, S. Iacovacci, P. Ricci, G. Gola, G. Candela, A.S. Sardo, R. De Angelis, C. Buzzoni, R. Capocaccia, Changes in life expectancy for cancer patients over time since diagnosis, J. Adv. Res. 20 (2019) 153–159, https://doi.org/10.1016/j.jare.2019.07.002.
- [2] C.P. Wild, E. Weiderpass, B.W. Stewart (Eds.), World Cancer Report: Cancer Research for Cancer Prevention, International Agency for Research on Cancer, Lyon (FR), 2020. PMID: 39432694.
- [3] F. Bray, M. Laversanne, H. Sung, J. Ferlay, R.L. Siegel, I. Soerjomataram, A. Jemal, Global cancer statistics 2022: GLOBOCAN estimates of incidence and mortality worldwide for 36 cancers in 185 countries, CA Cancer J. Clin. 74 (2024) 229–263, https://doi.org/10.3322/caac.21834.
- [4] A.B. Benson, A.P. Venook, M.M. Al-Hawary, L. Cederquist, Y.-J. Chen, K. K. Ciombor, S. Cohen, H.S. Cooper, D. Deming, P.F. Engstrom, J.L. Grem, A. Grothey, H.S. Hochster, S. Hoffe, S. Hunt, A. Kamel, N. Kirilcuk, S. Krishnamurthi, W.A. Messersmith, J. Meyerhardt, M.F. Mulcahy, J.D. Murphy, S. Nurkin, L. Saltz, S. Sharma, D. Shibata, J.M. Skibber, C.T. Sofocleous, E. M. Stoffel, E. Stotsky-Himelfarb, C.G. Willett, E. Wuthrick, K.M. Gregory, L. Gurski, D.A. Freedman-Cass, Rectal cancer, version 2.2018, NCCN clinical practice guidelines in oncology, J. Natl. Compr. Cancer Netw. 16 (2018) 874–901, https://doi.org/10.6004/inccn.2018.0061.
- [5] A. De Weerdt, A. Dendooven, A. Snoeckx, J. Pen, M. Lammens, P.G. Jorens, Prognosis and treatment of FOLFOX therapy related interstitial pneumonia: a plea for multimodal immune modulating therapy in the respiratory insufficient patient, BMC Cancer 17 (2017) 586, https://doi.org/10.1186/s12885-017-3576-y.

- [6] H.H. Kampinga, Cell biological effects of hyperthermia alone or combined with radiation or drugs: a short introduction to newcomers in the field, Int. J. Hyperth. 22 (2006) 191–196, https://doi.org/10.1080/02656730500532028.
- [7] A. Gadducci, S. Cosio, P.V. Lippolis, Hyperthermic intraperitoneal chemotherapy in the management of primary epithelial ovarian cancer: a debated issue for gynecologic oncologists, Anticancer Res. 42 (2022) 4659–4665, 10.21873/ anticanres.15970 %J Anticancer Research.
- [8] S.N. Koole, P.C. Schouten, J. Hauke, R.J.C. Kluin, P. Nederlof, L.K. Richters, G. Krebsbach, K. Sikorska, M. Alkemade, M. Opdam, J.H. Schagen van Leeuwen, H. W.R. Schreuder, R.H.M. Hermans, I.H.J.T. de Hingh, C.H. Mom, H.J.G. Arts, M. van Ham, P. van Dam, P. Vuylsteke, J. Sanders, H.M. Horlings, K.K. van de Vijver, E. Hahnen, W.J. van Driel, R. Schmutzler, G.S. Sonke, S.C. Linn, Effect of HIPEC according to HRD/BRCAwt genomic profile in stage III ovarian cancer: results from the phase III OVHIPEC trial, Int. J. Cancer 151 (2022) 1394–1404, https://doi.org/10.1002/ijc.34124.
- [9] G.C. van Rhoon, M. Franckena, T.L.M. ten Hagen, A moderate thermal dose is sufficient for effective free and TSL based thermochemotherapy, Adv. Drug Deliv. Rev. 163-164 (2020) 145–156, https://doi.org/10.1016/j.addr.2020.03.006.
- [10] J.C. Forster, W.M. Harriss-Phillips, M.J. Douglass, E. Bezak, A review of the development of tumor vasculature and its effects on the tumor microenvironment, Hypoxia (Auckland, N.Z.) 5 (2017) 21–32, https://doi.org/10.2147/hp.S133231.
- [11] R.D. Issels, Hyperthermia adds to chemotherapy, Eur. J. Cancer 44 (2008) 2546–2554, https://doi.org/10.1016/j.ejca.2008.07.038.
- [12] J. Crezee, N.A.P. Franken, A.L. Oei, Hyperthermia-based anti-cancer treatments, Cancers 13 (2021) 1240.
- [13] S. Eetezadi, R. De Souza, M. Vythilingam, R. Lessa Cataldi, C. Allen, Effects of doxorubicin delivery systems and mild hyperthermia on tissue penetration in 3D cell culture models of ovarian cancer residual disease, Mol. Pharm. 12 (2015) 3973–3985, https://doi.org/10.1021/acs.molpharmaceut.5b00426.
- [14] G.Y. Yi, M.J. Kim, H.I. Kim, J. Park, S.H. Baek, Hyperthermia treatment as a promising anti-cancer strategy: therapeutic targets, perspective mechanisms and synergistic combinations in experimental approaches, Antioxidants 11 (2022) 625.
- [15] L. Farzin, R. Saber, S. Sadjadi, E. Mohagheghpour, A. Sheini, Nanomaterials-based hyperthermia: a literature review from concept to applications in chemistry and biomedicine, J. Ther. Biol. 104 (2022) 103201, https://doi.org/10.1016/j. itherbio.2022.103201.
- [16] Z.S. Sayed, E.M. Hieba, H.A. Batakoushy, H.R.M. Rashdan, E. Ismail, S. M. Elkatlawy, A. Elzwawy, Cancer treatment approaches within the frame of hyperthermia, drug delivery systems, and biosensors: concepts and future potentials, RSC Adv. 14 (2024) 39297–39324, https://doi.org/10.1039/DARA06992G
- [17] S.A. Fahmy, E. Preis, A.A. Dayyih, M. Alawak, H.M. El-Said Azzazy, U. Bakowsky, T. Shoeib, Thermosensitive liposomes encapsulating nedaplatin and picoplatin demonstrate enhanced cytotoxicity against breast cancer cells, ACS Omega 7 (2022) 42115–42125, https://doi.org/10.1021/acsomega.2c04525.
 [18] C.M. Clavel, P. Nowak-Sliwinska, E. Păunescu, P.J. Dyson, Thermoresponsive
- [18] C.M. Clavel, P. Nowak-Sliwinska, E. Păunescu, P.J. Dyson, Thermoresponsive fluorinated small-molecule drugs: a new concept for efficient localized chemotherapy, MedChemComm 6 (2015) 2054–2062, https://doi.org/10.1039/ C5MD00409H.
- [19] C.M. Clavel, O. Zava, F. Schmitt, B.H. Kenzaoui, A.A. Nazarov, L. Juillerat-Jeanneret, P.J. Dyson, Thermoresponsive chlorambucil derivatives for tumour targeting, Angew. Chem. Int. Ed. 50 (2011) 7124–7127, https://doi.org/10.1002/ anie 201101133
- [20] J.W. Walton, J.M. Cross, T. Riedel, P.J. Dyson, Perfluorinated HDAC inhibitors as selective anticancer agents, Org. Biomol. Chem. 15 (2017) 9186–9190, https://doi. org/10.1039/c7ob02339a.
- [21] C.M. Clavel, E. Paunescu, P. Nowak-Sliwinska, P.J. Dyson, Thermoresponsive organometallic arene ruthenium complexes for tumour targeting, Chem. Sci. 5 (2014) 1097–1101, https://doi.org/10.1039/c3sc53185f.
- [22] C.M. Clavel, E. Paunescu, P. Nowak-Sliwinska, A.W. Griffioen, R. Scopelliti, P. J. Dyson, Modulating the anticancer activity of ruthenium(II)-arene complexes, J. Med. Chem. 58 (2015) 3356–3365, https://doi.org/10.1021/jm501655t.
- [23] S. Cabrera, F. Navas, A.I. Matesanz, M. Maroto, T. Riedel, P.J. Dyson, A.G. Quiroga, Versatile route to trans-platinum(II) complexes via manipulation of a coordinated 3-(pyridin-3-yl)propanoic acid ligand, Inorg. Chem. 58 (2019) 7200–7208, https://doi.org/10.1021/acs.inorgchem.9b00126.
- [24] A.D. McAdam, L.K. Batchelor, J. Romano-deGea, D. Vasilyev, P.J. Dyson, Thermoresponsive carboplatin-releasing prodrugs, J. Inorg. Biochem. 254 (2024) 112505, https://doi.org/10.1016/j.jinorgbio.2024.112505.
- [25] J. Quero, F. Ruighi, J. Osada, M.C. Gimeno, E. Cerrada, M.J. Rodriguez-Yoldi, Gold (I) complexes bearing alkylated 1,3,5-triaza-7-phosphaadamantane ligands as thermoresponsive anticancer agents in human colon cells, Biomedicines 9 (2021) 1848–1866, https://doi.org/10.3390/biomedicines9121848.
- [26] R.T. Mertens, S. Gukathasan, A.S. Arojojoye, C. Olelewe, S.G. Awuah, Next generation gold drugs and probes: chemistry and biomedical applications, Chem. Rev. 123 (2023) 6612–6667, https://doi.org/10.1021/acs.chemrev.2c00649.
- [27] Y.L. Lu, X.Y. Ma, X.Y. Chang, Z.L. Liang, L. Lv, M. Shan, Q.Y. Lu, Z.F. Wen, R. Gust, W.K. Liu, Recent development of gold(i) and gold(iii) complexes as therapeutic agents for cancer diseases, Chem. Soc. Rev. 51 (2022) 5518–5556, https://doi.org/10.1039/d1cs00933h.
- [28] C. Ratia, R.G. Soengas, S.M. Soto, Gold-derived molecules as new antimicrobial agents, Front. Microbiol. 13 (2022) 846959, https://doi.org/10.3389/ fmicb.2022.846959.
- [29] C. Hemmert, H. Gornitzka, C. Deraeve, J.-L. Stigliani, Current state of the art of gold complexes as antileishmanial agents, Coord. Chem. Rev. 528 (2025) 216408, https://doi.org/10.1016/j.ccr.2024.216408.

- [30] A. Tialiou, J. Chin, B.K. Keppler, M.R. Reithofer, Current developments of <i>N</i>i>-heterocyclic carbene Au(I)/Au(III) complexes toward cancer treatment, Biomedicines 10 (2022) 1417, https://doi.org/10.3390/biomedicines10061417.
- [31] A. Steinbrueck, M.L. Reback, C. Rumancev, D. Siegmund, J. Garrevoet, G. Falkenberg, A. Rosenhahn, A. Prokop, N. Metzler-Nolte, Quinizarin gold(I) Nheterocyclic carbene complexes with synergistic activity against anthracyclineresistant leukaemia cells: synthesis and biological activity studies, Chem. Eur. J. 31 (2025) e202404147, https://doi.org/10.1002/chem.202404147.
- [32] A. D'Amato, D. Iacopetta, J. Ceramella, R. Troiano, A. Mariconda, A. Catalano, M. Marra, C. Saturnino, C. Rosano, M.S. Sinicropi, P. Longo, Design, synthesis and biological evaluation of multitarget hybrid molecules containing NHC-Au(I) complexes and carbazole moieties, Eur. J. Med. Chem. 277 (2024) 116757, https://doi.org/10.1016/j.ejmech.2024.116757.
- [33] F. Bannwart, L.F. Richter, S. Stifel, J. Rueter, H.N. Lode, J.D.G. Correia, F.E. Kühn, A. Prokop, A new class of gold(I) NHC complexes with proapoptotic and resensitizing properties towards multidrug resistant leukemia cells overexpressing BCL-2, J. Med. Chem. 67 (2024) 15494–15508, https://doi.org/10.1021/acs. jmedchem.4c01117.
- [34] R.Z. Essa, Brianna, C.I. Yeo, S.-Y. Teow, Gold complexes and their molecular targets in colorectal cancer, J. Organomet. Chem. 1010 (2024) 123097, https://doi.org/10.1016/j.jorganchem.2024.123097.
- [35] H. Ghareeb, N. Metanis, The thioredoxin system: a promising target for cancer drug development, Chem. Eur. J. 26 (2020) 10175–10184, https://doi.org/10.1002/ chem.201905792.
- [36] M. Bian, R. Fan, S. Zhao, W. Liu, Targeting the thioredoxin system as a strategy for cancer therapy, J. Med. Chem. 62 (2019) 7309–7321, https://doi.org/10.1021/ acs.jmedchem.8b01595.
- [37] R. Visbal, V. Fernandez-Moreira, I. Marzo, A. Laguna, M.C. Gimeno, Cytotoxicity and biodistribution studies of luminescent Au(I) and Ag(I) N-heterocyclic carbenes. Searching for new biological targets, Dalton Trans. 45 (2016) 15026–15033, https://doi.org/10.1039/c6dt02878k.
- [38] A. Johnson, M.C. Gimeno, An efficient and sustainable synthesis of NHC gold complexes, Chem. Commun. 52 (2016) 9664–9667, https://doi.org/10.1039/ c6cc05190a.
- [39] A.M. Pizarro, R.J. McQuitty, F.S. Mackay, Y. Zhao, J.A. Woods, P.J. Sadler, Cellular accumulation, lipophilicity and photocytotoxicity of diazido platinum(IV) anticancer complexes, Chemmedchem 9 (2014) 1169–1175, https://doi.org/ 10.1002/cmdc.201402066.
- [40] O. Ekinci, M. Akkoç, S. Khan, S. Yaşar, C. Gürses, S. Noma, S. Balcıoğlu, B. Sen, M. Aygün, İ. Yılmaz, Synthesis and biological evaluation of Au-NHC complexes, Appl. Organomet. Chem. 36 (2022) e6811, https://doi.org/10.1002/aoc.6811.
- [41] A.A.A. Sulaiman, N. Casagrande, C. Borghese, G. Corona, A.A. Isab, S. Ahmad, D. Aldinucci, M. Altaf, Design, synthesis, and preclinical activity in ovarian cancer models of new phosphanegold(I)-N-heterocyclic carbene complexes, J. Med. Chem. 65 (2022) 14424–14440, https://doi.org/10.1021/acs.jmedchem.2c00737.
- [42] M. Mora, M.C. Gimeno, R. Visbal, Recent advances in gold-NHC complexes with biological properties, Chem. Soc. Rev. 48 (2019) 447–462.
- [43] I. Marmol, J. Quero, M.J. Rodriguez-Yoldi, E. Cerrada, Gold as a possible alternative to platinum-based chemotherapy for colon cancer treatment, Cancers 11 (2019) 780, https://doi.org/10.3390/cancers11060780.
- [44] A. Zweibaum, M. Bourel, H. Lestradet, J. Chretien, G. Richet, Differentiation of human colon-cancer cells - a new approach of colon-cancer, Bull. Acad. Natl Med. 177 (1993) 63–73.
- [45] S. Tu, R. Wai-Yin Sun, M.C. Lin, J. Tao Cui, B. Zou, Q. Gu, H.F. Kung, C.M. Che, B. C. Wong, Gold (III) porphyrin complexes induce apoptosis and cell cycle arrest and inhibit tumor growth in colon cancer, Cancer 115 (2009) 4459–4469, https://doi.org/10.1002/cncr.24514.
- [46] M.P. Chrysouli, C.N. Banti, N. Kourkoumelis, N. Panayiotou, G.S. Markopoulos, A. J. Tasiopoulos, S.K. Hadjikakou, Chloro(triphenylphosphine)gold(I) a forefront reagent in gold chemistry as apoptotic agent for cancer cells, J. Inorg. Biochem. 179 (2018) 107–120, https://doi.org/10.1016/j.jinorgbio.2017.11.004.
- [47] E. Abás, A. Bellés, A. Rodríguez-Diéguez, M. Laguna, L. Grasa, Selective cytotoxicity of cyclometalated gold(III) complexes on Caco-2 cells is mediated by G2/M cell cycle arrest, Metallomics 13 (2021) mfab034, https://doi.org/10.1093/ mtomes/mfab034
- [48] K.J. Barnum, M.J. O'Connell, Cell cycle regulation by checkpoints, Methods Mol. Biol. 1170 (2014) 29–40, https://doi.org/10.1007/978-1-4939-0888-2_2.
- [49] I. Marmol, M. Virumbrales-Munoz, J. Quero, C. Sanchez-De-Diego, L. Fernandez, I. Ochoa, E. Cerrada, M.J.R. Yoldi, Alkynyl gold(I) complex triggers necroptosis via ROS generation in colorectal carcinoma cells, J. Inorg. Biochem. 176 (2017) 123–133, https://doi.org/10.1016/j.jinorgbio.2017.08.020.
- [50] T.S. Reddy, S.H. Privér, R. Ojha, N. Mirzadeh, G.R. Velma, R. Jakku, T. Hosseinnejad, R. Luwor, S. Ramakrishna, D. Włodkowic, M. Plebanski, S. K. Bhargava, Gold(I) complexes of the type [AuL{κC-2-C6H4P(S)Ph2}] [L = PTA, PPh3, PPh2(C6H4-3-SO3Na) and PPh2(2-py)]: synthesis, characterisation, crystal structures, and in vitro and in vivo anticancer properties, Eur. J. Med. Chem. 281 (2025) 117007, https://doi.org/10.1016/j.ejmech.2024.117007.
- [51] J. Lu, A. Holmgren, The thioredoxin antioxidant system, Free Radic. Biol. Med. 66 (2014) 75–87, https://doi.org/10.1016/j.freeradbiomed.2013.07.036.
- [52] R. Gencheva, Q. Cheng, E.S.J. Arnér, Thioredoxin reductase selenoproteins from different organisms as potential drug targets for treatment of human diseases, Free Radic. Biol. Med. 190 (2022) 320–338, https://doi.org/10.1016/j. freeradbiomed.2022.07.020.
- [53] D.T. Lincoln, E.M. Ali Emadi, K.F. Tonissen, F.M. Clarke, The thioredoxinthioredoxin reductase system: over-expression in human cancer, Anticancer Res. 23 (2003) 2425–2433.

- [54] R. Uson, A. Laguna, M. Laguna, Tetrahydrothiophene gold(I) or gold(III) complexes, Inorg. Synth. 26 (1989) 85–91.
- [55] A. Raba, M.R. Anneser, D. Jantke, M. Cokoja, W.A. Herrmann, F.E. Kühn, Facile and scalable preparation of 2-imidazolylpyridines, Tetrahedron Lett. 54 (2013) 3384–3387, https://doi.org/10.1016/j.tetlet.2013.04.060.
- [56] E. Garcia-Moreno, S. Gascon, M.J. Rodriguez-Yoldi, E. Cerrada, M. Laguna, S-propargylthiopyridine phosphane derivatives as anticancer agents: characterization and antitumor activity, Organometallics 32 (2013) 3710–3720.
- [57] J. Quero, J.C. Royo, B. Fodor, M.C. Gimeno, J. Osada, M.J. Rodríguez-Yoldi, E. Cerrada, Sulfonamide-derived dithiocarbamate gold(I) complexes induce the apoptosis of colon cancer cells by the activation of caspase 3 and redox imbalance, Biomedicines 10 (2022), https://doi.org/10.3390/biomedicines10061437.